IPP-Report

Max-Planck-Institut für Plasmaphysik

Otto J.W.F. Kardaun

Reflections on plasma confinement and operational boundaries, ensuing from Experimental Thermonuclear Installation – TOKAMAK-20 – Preliminary Study

IPP 2017-05
November 2017

Reflections on plasma confinement and operational boundaries[1], ensuing from 'Experimental Thermonuclear Installation – TOKAMAK-20 – Preliminary Study'

National Committee for the Utilization of Atomic Energy, Soviet Ministry, USSR

authored by

V.V. Alikaev, V.A. Glukhikh, Y.N. Dnestrovskij, D.P. Ivanov,
B.B. Kadomtsev, S.B. Mirnov, N.A. Monoszoh,
V.S. Mukhovatov, G.N. Popkov, N.N. Semashko, V.S. Strelkov,
C.F. Churakov, V.D. Shafranov; translated by I.N. Sviatoslavsky

June 1975

UWFDM-129

0. Summary Aspect of the Preliminary Study

The main plasma parameters foreseen for the circular T–20 device, designed with 24 toroidal field coils accommodating a stored magnetic energy of 6 GJ, are given in the Appendix.

For this device, both neutral-beam injected (NBI) and radio frequency (RF) heating has been planned, consisting of (a) a positive neutral beam injection system, which would inject in total 60+50 = 110 MW into the plasma, with 80 keV and 160 keV particle energy, respectively (total power supply needed: 400 MW); (b) an RF system (ECRH, LH or ICRH), to inject another 60 MW into the plasma, with an additionally needed total power supply of 200 MW.

Both a hydrogen phase ($\simeq 10^4$ pulses) and a D+T phase was foreseen ($\simeq 10^5$ pulses). During D+T burning phase, at least some 60 MW absorbed auxiliary heating power was considered to be necessary to sustain the plasma temperature, in the presence of about 20 MW alpha-particle heating, while assuming an energy confinement time $\tau_E = 2\,\mathrm{s}$. Also the possibilities of attaining $\tau_E = 1\,\mathrm{s}$, with $Q \simeq 1$ at $T_e \simeq 10$ keV and $Q = 0.3$ at $T_e \simeq 5$ keV, were mentioned in this report (see section IV, 'Plasma heating methods', in [1], after the sentence: 'The planned complex of plasma heating has many possibilities for experimenting, depending on the attained $n\tau_E$').

The machine size and expected performance of T–20 was maintained to be suitable for a uranium or thorium hybrid reactor, and was stated to be at the same time an intermediate step toward a reactor which is based on nuclear fusion only.

1. Hindsight Reflection

It is of some interest to look, with the benefit of hindsight, at the performance prediction of such a tokamak device several decades later.

In 1975, neither the confinement degradation with strong additional heating power [26] nor the Murakami–Hugill–Greenwald–Borrass density limit, see [7, 29, 30, 86], were known, and also the H–mode regime [118] was not yet discovered. First of all, for the T–20 reference design, $n/n_{Gr} \simeq 1$, with $n_{Gr} = I_p/(\pi a^2)$ the Greenwald density, which is not far from $n/n_{Gr} \simeq 0.85$ foreseen as a reference scenario in ITER FEAT with sufficiently centralised (e.g. pellet) particle fueling. Secondly, two commonly used empirical H–mode scalings are ITER–89P for L–mode [122] and IPB–98(y,2) for ELMy H–mode [44]. They give for T–20 at (20) 50 MW power across the

[1] Technical IPP report 2017-05, prepared by Otto J.W.F. Kardaun, July 2007, revised during period July 2008 – Winter 2014, with additional text: Autumn 2016 - Autumn 2017, Garching bei München.

Table 1: Dimensionless and engineering plasma parameters (four tokamaks)

		β_p	β_t	β_N	$\langle B_p\rangle$	$\rho_{*,p,ion}$	ν_*	R	a	b/a	I_p	B_t	$\bar{n}_e$	$\tau_{E,th}$
'observed'	Tore-Supra	0.2	0.3 %	0.5	0.42	1.5 %	20 %	2.35	0.78	1	1.6	3.6	5.0	0.75
	TFTR	0.8	0.4 %	1.2	0.37	4.0 %	6 %	2.5	0.85	1	1.45	5.1	4.3	0.435
'required'	T–20	1.0	3.4 %	4.0	0.63	2.0 %	0.33 %	5.0	2.0	1	6	3.5	5	2.0
	ITER FEAT	0.5	2.3 %	1.6	1.1	0.7 %	1.9 %	6.2	2.0	1.7	15	5.3	10	3.66

last closed flux-surface the values $\tau_E = (0.8)\ 0.5$ s and $\tau_E = (1.5)\ 0.82$ s, respectively. According to a later developed scaling, 'Chengdu–2006' [53], designed to be more accurate for describing the confinement time near Greenwald limit, while taking the plasma shape into account by using q_{95}/q_{cyl} as a proxy variable for the triangularity, the corresponding values are $\tau_E = (1.2)\ 0.6$ s, respectively, while two recently obtained interaction-type scalings, specified by Eqs (1) and (2) in the present report, both give $\tau_E = (1.3)\ 0.65$ s

Meanwhile, during the nineties of the last century, $\tau_E = 0.12$ s has been achieved in TFTR ($V = 40$ m^3; $P_L = 20$ MW; $I_p = 1.5$ MA) during super-shot / H–mode (# 78174 , t=3.7 s.) and $\tau_E = 0.19$ s was attained in Tore Supra ($V = 30$ m^3; $P_L = 3.5$ MW, $I_p = 1.6$ MA) during L–mode (# 23427, t=6.57 s.).[2] According to the very crude approximation $\tau_E \sim I_p^{(2/3)} V^{(2/3)} P_L^{-(2/3)}$ this would have led to predictions 0.75 s (super-shot / H–mode, from TFTR) and 0.435 s (L–mode, from Tore Supra), respectively, for T–20 at $P_L = 50$ MW. For a further enquiry, the reader is referred to Table 1, in which the first two lines are observations from actual discharges (in Tore Supra and in TFTR, respectively). The second two lines correspond to values *as required or anticipated* according to the pre-set design goals in T–20 ($\tau_E = 2$ s, $W_{th} = 100$ MJ, $P_L = 50$ MW) and in ITER FEAT ($\tau_E = 3.66$ s, $W_{th} = 320$ MJ, $P_L = 87$ MW), respectively. Table 1 displays, on the left-hand side, the following plasma parameters (most of which are dimensionless): (a) $\beta_p = 2\mu_0[(2/3)W_{th}]/\langle B_p\rangle^2 V$, (b) $\beta_t = 2\mu_0[(2/3)W_{th}]/B_t^2 V$, (c) $\beta_N = 100(aB_t/I_p[\mathrm{MA}])\beta_t$, (d) $\langle B_p\rangle = \mu_0 I_p/L$, (e) $\rho_{*,p,ion} \sim (\sqrt{M_{\mathrm{eff}}}/Z)(\sqrt{\langle T\rangle}/I_p)$ and (f) $\nu_* = 0.01\langle n_e\rangle_{19}\, q_{95} R Z_{\mathrm{eff}} (R/a)^{1.5}/\langle T\rangle^2$.

For the definitions of β and ν_* see e.g. [77] and for the normalised poloidal ion gyro-radius[3] $\rho_{*,p,ion}$ see [11, 44] and [56, Ch 7.1, Case 1D]. As $\langle B_p\rangle L = \mu_0 I$, we used $\rho_{*,p,ion} = r_{*,p,ion}/(L/2\pi)$ instead of $r_{*,p,ion}/a$. The symbols have their usual meaning: W_{th} is the stored thermal plasma energy, and $\kappa_a = V/(2\pi R \pi a^2)$. It is noticed that $\langle B_p\rangle = \mu_0 I_p/L$, with L the contour length of the last closed flux-surface, and that $\langle T\rangle$ [keV] $= W_{th}$ [MJ]$/(4.8 \times 10^{-3}\langle n_e\rangle_{19} V)$. On the right-hand side, Table 1 contains three corresponding global plasma-physics variables: plasma current I_p [MA], toroidal magnetic field on axis B_t [T] and the line-averaged central density $\bar{n}_e$ [10^{19} m^{-3}]. (In the present report we often use n as abbreviation for $\bar{n}_{e,20}$.) The last column of this table exhibits the (observed or projected) thermal energy confinement time τ_E [s].

From this table one can see that the required discharge parameters of the envisioned devices combine a low value of ν_* with a low value of $\rho_{*,p,ion}$. While the 'observed' and 'required' values

[2] Parameters of two discharges made available to the international H– and L–mode global confinement databases.

[3] For an (isotropic) Maxwellian velocity distribution function, the poloidal (ion) gyro-radius $r_{*,p,ion} = \frac{Mv_\perp}{ZeB_p}$ (with $v_\perp \sim \mathrm{N}_2(0, \sigma^2)$ and $\sigma^2 = kT/M$), is distributed as $\frac{\sqrt{MkT}}{ZeB_p}\chi_2$, where χ_2 is the standard 'Rayleigh distribution' with mode 1, mean $\sqrt{\pi/2} \simeq 1.25$ and root mean square $\sqrt{2}$. Also, $r_{*,p,ion} = v_\perp/\omega_c$ with ω_c the cyclotron frequency, as opposed to the Larmor (precession) frequency $\omega_L = \frac{1}{2}\omega_c$, see [2,23,25,44,63]. The thermal ion speed perpendicular to the magnetic field has been estimated by $v_\perp = \sqrt{\frac{ckT}{M}}$ with $c = 2$ instead of $c = 1$, see [9,37]. (It is noted that the median velocity $\langle v_\perp\rangle_{med}$, corresponding to $c = 2\ln 2$, has the attractive property of being equivariant under monotonic transformations, and therefore $\langle v_\perp\rangle_{med} = \sqrt{\langle v_\perp^2\rangle_{med}}$.)

of β_p are similar, the observed values of β_t are lower than the required ones, the latter of which are, with a reasonable uncertainty margin, predicted by existing confinement time scaling(s), see e.g. [53] and Annex 1 in the present report. From the third column in Table 1, it appears that, unlike for ITER FEAT, for T–20 the projected value of β_N is notably higher than the value β_N actually attained in TFTR and Tore Supra.

2. Afterthought

In Fig. 1^A the plasma performance variable $\beta_N = 100(aB_t/I_p)\beta_t$ is represented vertically, whereas along the horizontal axis the machine design parameter $\langle B_p \rangle = \mu_0 I_p/L$ is plotted, normalised by the value foreseen in ITER FEAT and displayed on a logarithmic scale.[4] The bulk of the points are the observed values for standard ELMy H–mode restricted to D into D, i.e. pure deuterium plasmas from 9 machines (ASDEX, AUG, C–MOD, DIII–D, JET, JFT–2M[5], JT–60U, PDX, TdeV). The standard dataset as settled around 2007 [53], of the international tokamak confinement database DB4 [110], following earlier activity by six tokamak teams (see e.g. [54,111]), has been used here, while applying the following three additional restrictions: (1) $1.6 < q_{cyl} < 3.0$, (2) $0.98 < \kappa_a < 2$, (3) $2.0 < R/a < 5.0$, with $q_{cyl} = 5(B_t/I_p)(a^2\kappa_a/R)$. While excluding the spherical tokamaks as well as bean-shaped PBX–M, these restrictions tailor the dataset to standard operation for conventional aspect-ratio tokamaks.

The labeled points are the parameters, 'as expected' for standard inductive operation, from several conceptual devices[6] (in increasing order with respect to $\langle B_p \rangle$): JT–60SA (2008), T–20 (1975), INTOR (1980-1987), ITER FEAT (2003) [r], ITER FEAT (2003), ITER FDR (1998), FIRE (2000), and BPX (1992). For definiteness and ease of reproducibility, the predicted values for β_N according to $H_{98}(y,2)$ are shown. (A variation of the plot is shown in Fig. 13.) Although the original nominal value of the T–20 design ($\tau_E = 2\,$s) has been rather optimistic with respect to the expected β_N performance, it appears that the point prediction according to $H_{98}(y,2)$, 0.75 s, leads to a combination ($\langle B_p \rangle$, β_N) in this plot that is closer to (in fact, within the boundary of) the observed –regular H–mode– data than that of several of the other machines that were designed more than two decades later.

While using the same dataset and the same horizontal axis as in Fig. 1^A, the vertical axis in Fig. 1^B displays, on a logarithmic scale, $(n/n_{Gr})/0.838$, with $n_{Gr} = I_p\,[\mathrm{MA}]/\pi a^2$. (The normalisation 0.838 corresponds to the reference value for ITER FEAT.) Since fusion power output increases with the plasma density, at constant temperature[7], the vertical axis represents in this figure a kind of plasma performance variable. It is noted that, with the exception of JT–60SA and BPX, the design point of T–20, despite its early setting, is also here closer to the bulk of the existing data than the reference points of the other machines. In both figures, the slopes of the tilted lines are approximately -1, and suggest the relationships $\beta_{N,max}\langle B_p \rangle \simeq 1.2$ and $n/n_{Gr,max} \sim \langle B_p \rangle^{-x}$, for some $3/4 < x < 5/4$, respectively.[8] The value of $\beta_{N,max}$ is clipped at

[4] Zero on the horizontal axis corresponds to the average poloidal magnetic field in ITER FEAT, which is 1.11 T.

[5] For JFT–2M the same factor for the isotope effect has been used as in Ref. [53].

[6] The following sources have been utilised for reference plasma parameters: [43, 49, 72, 77, 79, 119]. Slightly conservatively, for JT–60SA [100], #4-1 (ITER-like-shape inductive scenario) from Ref. [45, 49] has been chosen here, and, from [79], $V = 58\,\mathrm{m}^3$ has been used for BPX, for which a distinction is made between 'minimum' (m) and 'standard' (s) performance, as specified in [79, Table 2.3].

[7] In fact, at high density (where $T_i \simeq T_e$) and for T_e (near $x = r/a \simeq 1/3$) around 10 keV, $P_{fus} \sim n_e^2 T_e^{2.5}$, see [52]. A physically more accurate global performance criterion is given in [20].

[8] Possibly, not all machines provided already their highest normalised density discharges and, except for JET and AUG, not any pellet-refueled discharges are presently included in the standard confinement dataset.

Table 2: $1.2/\langle B_p\rangle$ (median and upper 90% quantile for conventional aspect-ratio tokamaks)

	ASDEX	AUG	C-MOD	DIII-D	JET	JFT-2M	JT-60U	PDX	TdeV
Q50	6.1	4.0	1.6	3.8	3.0	8.8	3.6	6.1	6.2
Q90	6.6	4.8	1.7	4.7	6.1	9.0	6.0	6.7	6.2

Table 3: 98% upper quantiles of (a): $\beta_N\langle B_p\rangle/1.2$, (b): $\beta_N/(4\times l_i)$, and (c): $2\times(n/n_{Gr})\langle B_p\rangle$ (for various tokamaks)

	ASD	AUG	C-MOD	DIII-D	JET	JFT-2M	JT-60U	PDX	TdeV	NSTX	MAST
$\beta_{N,max}\langle B_p\rangle/1.2$	0.4	0.7	0.9	0.75	0.75	0.22	0.3	0.35	0.17	1.15	0.53
$\beta_{N,max}/(4\times l_i)$	0.5	0.8	0.3	1.0	0.7	0.65	0.15	0.5	0.22	–	–
$2\times(n/n_{Gr})\langle B_p\rangle$	0.2	0.6	0.95	0.9	0.9	0.15	0.35	0.4	0.17	0.5	0.3

$e^{1.25}\simeq 3.5$. In one device one can vary $\langle B_p\rangle$ by changing I_p as well as L.[9] As an approximate indication of the maximum achievable β_N, in Table 2 the 50% and 90% quantiles of $1.2/\langle B_p\rangle$ have been displayed for the tokamaks included in the standard ELMy dataset mentioned above. (Values of β_N above Q_{90} are to be considered as a high-β discharge for that device.) Table 3 displays, for the data as provided to the confinement database and included in the standard dataset, 98% upper quantiles, i.e. 'almost the maximum attained values' for the following three cases: (a) of $\beta_N\langle B_p\rangle/1.2$, (b) of[10] $\beta_N/4l_i$ and (c) of $2\times(n/n_{Gr})\langle B_p\rangle$ for each of the tokamaks. In case (a), high values less than 1.0 are obtained by the ITER-similarly shaped C–MOD, AUG, DIII–D and JET devices. It is noted that the approximate relation $\beta_N\langle B_p\rangle\leq 1.2$ corresponds to $W_{th}[\mathrm{MJ}]\leq 1.2\times\frac{3}{64\pi^2}\times B_t(L/a)V\simeq 0.03B_t\kappa_a^{0.6}V$, while $\beta_t\leq c$ would correspond to $W_{th}[\mathrm{MJ}]\leq c\times\frac{30}{16\pi}\times B_t^2V$, whereas a simplified Troyon-type β-limit [113,123] (based on ideal MHD stability theory), $\beta_N\leq c'$, would entail $W_{th}[\mathrm{MJ}]\leq c'\times\frac{3}{64\pi^2}\times B_t\langle B_p\rangle(L/a)V$.

Not all tokamaks in Table 3 obtained standard H–mode plasmas at the maximum value of $\beta_N\langle B_p\rangle$ as suggested by the boundary in Fig. 1, and it may be worthwhile to remind the casual reader that Fig. 1 does not represent a universal scaling, among others because $\beta_{N,max}$ depends in addition on heating power and possibly also, to some extent, on the type of plasma heating. Data from the two spherical tokamaks MAST and NSTX, when added to Fig. 1, occur at high values of β_N and at low values of $\langle B_p\rangle$, such that the approximate straight line becomes more a quadratic-like boundary (on a logarithmic scale), while the empty space for the designed experiments is somewhat increased, see Fig. 13. Estimation of the number of existing tokamaks that have performed discharges in the empty ('right-upper') corner of this plot is not possible using the present dataset, at least not without invoking (somewhat artificially) a Poisson-type probabilistic model, as used, for instance, in [21,106].

For case (b), the variation is somewhat larger than for case (a), while for case (c) one can

[9] In absence of the plasma surface area $S\simeq 2\pi R_{geo}L$ being explicitly available in confinement DB1 to DB4v5, $L=2\pi a\kappa^{1-0.85\ln k}(1+\delta)^{-0.12}(1+a/R)^{-0.05}$ (with $\kappa=b/a$), based on a regression fit from power threshold DB [93] has been used as a simple approximation for all existing conventional aspect-ratio tokamaks (except for PBX–M) as well as for the projected devices (including FIRE).

[10] The plasma internal inductance ('peaking factor of the current profile'), l_i, has been estimated by using beili2 - beimhd as provided in DB4v5 [110]; its detailed implementation may vary somewhat between the various tokamaks, see [76] and [68] (Appendix). Existence region of achievable L– and H–mode discharges in (l_i, q_{eff})-plane (with q_{eff} depending on plasma shape as well as on $\beta_p+l_i/2$) is given for JT–60 Upgrade in [22,80].

see that the highest normalised densities (close to 1.0) were obtained by C–MOD, DIII–D and JET. In the right part of this table, the corresponding values, inasfar as available, for the tight aspect-ratio NSTX and MAST machines ($R/a \simeq 1.25$) have been added. For NSTX one can see a rather high value of β_N (1.15) and a rather low Greenwald fraction (0.5). Anyhow, the 'required' values for ITER FEAT (2003) are $\beta_N \langle B_p \rangle / 1.2 = 1.5\,\mathrm{MA/m}$ and $2 \times (n/n_{Gr}) \langle B_p \rangle = 1.85\,\mathrm{m}^{-2}$, respectively[11].

In Fig. 2, for comparison, the same variables are plotted as in Fig. 1, but now for the standard L–mode dataset while the same three additional selection criteria have been applied as for ELMy H–mode above. One can see from Fig. 2^A that the attainable values of β_N are, as expected (for $\langle B_p \rangle \gtrsim 0.5$ at least about 40%) lower than those for ELMy H–mode. The upper boundary satisfies to a good approximation again the relation $\beta_{N,max} \sim \langle B_p \rangle^{-1}$, even though for L–mode there is a clearer empty region between the observed maximal values of β_N and the boundary drawn by a straight line.

Obviously, Figs 1 and 2 have to be considered as 'existence diagrams for standard ELMy H–mode' exhibiting an improvement of the traditional β-limit and of the density limit only insofar as a representative set of the actually available discharges have been provided to the confinement database by the nine conventional aspect-ratio machines from Table 3, during the period 1982–2006. Note that this standard ELMy H–mode dataset has been devised to derive confinement-time scalings for standard (type I, type III) ELMy H–mode. Hence, discharges with beta degradation due to NTM's have been omitted, and neither discharges with NTM stabilisation through current drive [35, 70] nor long-pulse high β_p [48], or so-called 'improved' H–mode scenario, discharges [35, 107] are included here. From Fig. 2^B one notices that apparently the density limit for L–mode is different than for ELMy H–mode; the upper boundary satisfies $n/n_{Gr,max} \sim \langle B_p \rangle^{-y}$, for $1/4 \lesssim y \lesssim 1/2$, and several of the envisioned devices are closer to the bulk of the data than in the case of ELMy H–mode.

Based on a B_t-scan in L–mode, in [85, 86] it is maintained that, whereas $n_{Gr} = I_p/(\pi a^2)$ is more an edge than a central density limit (see also [30,64]), $\bar{n}_e \leq 0.25 B_T^{1.35}$ describes the attainable density boundary better than classical Greenwald limit n_{Gr}. Using the same dataset as before and replacing n_{Gr} by $B_t^{1.35}$ in Fig. 2 leads to a more horizontal boundary. This, however, does neither apply to Fig. 1 (H–mode), nor to the situation when $\langle B_p \rangle$ on the horizontal axis is replaced by RB_t. (Graphs not shown for simplicity of exposition.)

Annex 1. (Empirical scalings of plasma stored energy)

In Fig. 11 a rough impression is given of the deviations from the $\mathrm{H}_{98}(y, 2)$ scaling (on a logarithmic scale) as a function of both $\ln(B_t/\langle B_p \rangle)$ and $\ln(B_{max}/B_{min} - 1)$. The plot has been made using the non-parametric regression procedure PROC LOESS implemented in the statistical package SAS [94], and suggests that some improvement of the $\mathrm{H}_{98}(y, 2)$ 'Princeton/IPB' confinement-time scaling should be feasible. In fact, the H_{06}(dd,y) 'Chengdu' ELMy H–mode scaling [53] is an attempt in that direction. It describes the roll-over of the confinement time with respect to n/n_{Gr}, and includes a dependence on plasma shape, the latter being expressed by $F_{sh} = q_{95}/q_{cyl}$ with q_{cyl} as defined above. Moreover, by concentrating on D into D discharges only, it disentangles interaction effects of the isotope species with other plasma parameters, for instance (possibly) with $P_{L'}/\bar{n}_e V$ (see [54]). Its influence on ITER FEAT (2003) performance has been analysed in detail in [46], and a comparison with pellet fueled discharges at ASDEX Upgrade has been made in [65]. For conventional aspect-ratio devices it constitutes an improvement over the $\mathrm{H}_{98}(y, 2)$ scaling. However, in

[11] Dimensions are given replacing magnetic induction B by magnetic field H, or assuming μ_0 to be dimensionless, see also Figs 1, 2 and 13.

the 2006 scaling, the quadratic aspect-ratio dependence had been included in a rough and ready fashion. As shown in [57,67,115], the spherical tokamaks exhibit an I_p and B_t dependence that is different from what is generally observed in conventional tokamaks.[12] Therefore, the following refinement of the H_{06}(dd,y) scaling has been derived more recently, using weighted regression routine from SAS/PROC REG [94]. It is based on almost the same selection rules and a very similar D into D 'standard' dataset[13], as in 2006, with the very small COMPASS machine excluded and tuned to the medium to high density regime by applying the restriction $n/n_{Gr} > -\ln\ln(10) = -0.834$ (data from ASDEX, AUG, ALC C–MOD, DIII–D, JFT–2M, JT–60U, JET, PDX, PBX–M, TdeV, TFTR, MAST and NSTX[14]). The scaling reads

$$\frac{W_{th}}{87.7\,\mathrm{MW}} = c_{14} \times (I_p B_t)^{0.725} P_{L'}^{0.325} R_{geo}^{1.8} \kappa_a^{0.16-0.33\ln(\kappa_a)} F_A^{0.32-0.27\ln(F_A)} F_{sh}^{1.32} q_{cyl}^{-0.31-0.2\ln(q_{cyl})+0.58\ln(F_A)} (n/n_{Gr})^{-0.05-0.36\ln(n/n_{Gr})} \left(\frac{P_{L'}}{n^2 V}\right)^{-0.0225\ln\left(\frac{P_{L'}}{n^2 V}\right)} \text{[s]} \qquad (1)$$

where[15] $F_{sh} = \frac{q_{95}}{q_{cyl}}$, n stands for $\bar{n}_{e,20}$, and[16] $F_A = \frac{2}{R/a-1} = \frac{B_{max}-B_{min}}{B_{min}}$. The estimated intercept $c_{14} \simeq e^{1.2} \simeq 3.3$, and the unweighted RMSE ($\equiv \hat{\sigma}_{unweighted}$) from the fitted regression surface is 14.9%. As in [53], ITER FEAT units are used throughout[17] and the prediction at the standard ITER operating point is $W_{th} = 285 \times (M_{\mathrm{eff}}/2.5)^{0.2}$ MJ, which is, within a few percent, similar to the point prediction according to H_{06}(dd,y). From the exponent of q_{cyl}, one can see that for higher aspect ratio $A = R/a$, i.e. for a lower value of F_A, the exponent of B_t decreases while the exponent of I_p increases. All coefficients of the 'higher-order' (i.e. quadratic and interaction) terms are statistically significant in the sense that their estimates are larger, in absolute value, than 2 times (in our case more than about 6 times[18]) their standard deviation. The last interaction term in Eq. (1) indicates that the effective exponent of $P_{L'}$, $\alpha_{P_{L'}}$(eff), decreases with increasing heating power and hence reflects a feature of offset-linear scalings, see e.g. [12,109,122].

[12] The expression 'generally' is used here in view of an early, somewhat puzzling, strong ($B_t^{0.6}$) dependence in a scaling for six conventional tokamaks based on ordinary least squares, which is in contrast to a restricted dependence based on single machine scans ($B_t^{0.15}$) in [12], and also to the essentially unrestricted OLS fit of $H_{98}(y,2)$ ($B_t^{0.15}$) in [44]. In all these cases, the sum of the I_p and B_t exponents is approximately constant. Whether this sum, related to the collisionality dependence, is stronger for low aspect-ratio machines is still an interesting and somewhat open question. For further experimental information the reader is referred to [115].

[13] The following specific modifications have been made. Omitted are from JET, shot< 30000 (period November 1986 – September 1990, 29 time slices), and included are from AUG, iseq='PELLET' (period April 1998 – July 2003, 22 time slices). Moreover, in order to reduce sensitivity to outlying observations, data with $|H_{98y2}| > 0.5$ have been trimmed to $|H_{98y2}| = 0.5$, while in [53] data for which $|H_{98y2}| > 0.4$ have been 'deleted', i.e. omitted while deriving the scaling; for corresponding general theory, see [99].

[14] For the relative weighting scheme applied to the observations ('time-slices') that have been contributed by each of the tokamaks, see Appendix.

[15] Inclusion of the plasma shape factor F_{sh} as in [53] reflects to some extent also the decreasing width of the sawtooth inversion radius with increasing q_{95}, see [104].

[16] Usage of factor F_A here, instead of $A = R/a$, has been motivated by investigation [108] on the heating power required for the L–mode to H–mode transition.

[17] such that logarithms of plasma parameters in Eqs (1) to (3) are zero at

$$(I_p, B_t, P_{L'}, n/n_{Gr}, R_{geo}, a_{min}, V, \kappa, \kappa_a, q_{95}, q_{cyl}) = (15\,\mathrm{MA}, 5.3\,\mathrm{T}, 87.7\,\mathrm{MW}, 0.838, 6.2\,\mathrm{m}, 2\,\mathrm{m}, 831\,\mathrm{m}^3, 1.86, 1.74, 3.0, 2.12)$$

while $(F_A, F_{sh}) = (\frac{2}{(R/6.2)(2.0/a)-1}, \frac{q_{95}/3.0}{q_{cyl}/2.12})$ and $P_{L'}/S = \frac{P_{L'}[\mathrm{MW}]}{87.7} / \frac{S[\mathrm{m}^2]}{680}$.

[18] according to the weighted least-squares algorithm implemented in SAS/PROC REG, where multiplying all weights by a fixed constant does not influence the statistical significance of the regression coefficients, see also [61,89,116]. If the uncertainty in the regression coefficients would be inflated (as an exercise at this occasion) by an additional factor $\frac{\hat{\sigma}_{unweighted}}{\hat{\sigma}_{weighted}} \simeq 1\frac{4}{9}$, then the estimate 6 std. dev. would drop to about 4 std. dev.

Fitting 'perestroika-type' (e.g. cusp-like) response surfaces to combined (H– and L–mode) subsets of the data, see e.g. [50, 51], is appealing from a fundamental point of view. Full concrete evaluation is an exacting task since an inductive search of the basic control parameters is needed and estimation theory is yet under development. It is possibly still somewhat too ambitious at present for reliable and robust extrapolation to (differently sized, shaped, and conditioned) large future devices, in spite of a relatively recent, software implementation (based on maximum likelihood estimation) in R, the latter being explicated in [28], and of a, slightly legerdemain, practical application to medical data described in [10].

Therefore, in the context of the present report, since $\alpha_{P_{L'}}(\mathrm{eff})$ is of practical relevance, several similar interaction terms have been inquired along the approach described above. This led, autumn 2016 – summer 2017, to the following interaction-type scaling for the thermal stored energy, provisionally denoted here as H_{16}(dd,y;th):

$$\frac{W_{th}}{87.7\,\mathrm{MW}} = c_{16} \times (I_p B_t)^{0.6-0.04\ln(P_{L'}/S)} P_{L'}^{0.25} R_{geo}^{2.07} \kappa_a^{0.125-0.75\ln(\kappa_a)} F_A^{0.585-0.28\ln(F_A)} F_{sh}^{0.78} q_{cyl}^{-0.47+0.70\ln(F_A)} (n/n_{Gr})^{-0.125-0.2\ln(n/n_{Gr})} \left(\frac{P_{L'}}{n^2 V}\right)^{-0.04\ln\left(\frac{P_{L'}}{n^2 V}\right)} \;[\mathrm{s}] \qquad (2)$$

($N_{tok} = 13$, $N_{obs} = 2963$, RMSE=14.5%), with $c_{16} \simeq 2.6$. The parameter S denotes the plasma surface area; in accordance[19] with [77], $S = 680\,\mathrm{m}^2$ has been utilised as reference value for ITER FEAT. As before, the coefficients of all leading interaction terms are at least 6 standard deviations different from zero.

Eq. (2) shows (among others) a saturation of the confinement time with respect to κ_a. This dependence is weak, 0.125, at ITER FEAT reference value $\kappa_a = 1.74$. One can infer also, however, that (e.g. for JFT–2M) at $\ln(\kappa_a) \simeq \ln(1.3/1.74) = -0.3$, the local log-linear κ_a exponent (here at constant values of q_{cyl} and q_{95}) is close to $0.125 + 2 \times 0.75 \times 0.3 = 0.6$. This is in reasonable agreement with the positive κ dependence (there at constant I_p and B_t) of ELMy and ELM-free H–mode analysed earlier in [74]. Table 4 shows the weighted averages as well as the variation of the main combinations of plasma parameters that occur in Eq. (2). While some of them (such as R_{geo}) are fixed during the design phase, others can still be varied (over a certain range), once a machine is constructed. With respect to the plasma shaping factor $\ln F_{sh} = \ln(q_{95}/q_{cyl})$, it is noted that low values (between −0.3 and −0.1 in ln ITER FEAT units) have been obtained by low k_a devices ASDEX, JT–60U and PDX, and high values (between 0.45 and 1.1) by MAST, NSTX (at low $A = R/a$) as well as by PBX–M (at high $A = R/a$).

Inclusion of the interaction term $(I_p B_t)^{0.6-0.04\ln(P_{L'}/S)}$ in Eq. (2), while omitting the term $q_{cyl}^{-0.2\ln(q_{cyl})}$ (which has lost significance), leads to modest estimates for the prediction at the standard operating point in ITER ($W_{th} = 230\,\mathrm{MJ} \times (M_{\mathrm{eff}}/2.5)^{0.2}$), which is close to the lower bound of the 95% interval estimate from 2002 [55] ($W_{th} = \tau_{E,th} P_{L'} = 237\,\mathrm{MJ}$), as well as to the point prediction from the offset non-linear scaling in [109] ($W_{th} = 244\,\mathrm{MJ}$). It is therefore of specific interest to investigate whether a physical reason exists for the occurrence of this interaction term –i.e., between $I_p B_t$ and $P_{L'}/S$– in the DB4v5 'standard' confinement dataset, which does include carbon divertor, but not any ILW discharges from JET (for a comparison, see e.g. [8]). The ICRH heated discharges from Alcator C–mod do have a relatively weak $P_{L'}$ exponent. However, omitting them from the standard dataset does not notably change this interaction term.

Sometimes, for simplicity, $W_{tot} = W_{th} + W_{fp} = \frac{2}{3} W_{MHD} + \frac{1}{3} W_{DIA}$ is used instead of W_{th}. Using the same standard dataset (and weighting scheme) as above, an auxiliary scaling for the

[19] in DB4v5, the range of S for AUG (with $S = \frac{1}{16} S_{\mathrm{ITER}}$), is $40\ \mathrm{m}^2 < S < 44\ \mathrm{m}^2$

fraction of fast particles, similar in type to Table II in [54] (based on six tokamaks), is given[20] by

$$W_{tot}/W_{th} = C_{aux}(I_pB_t)^{0.115+0.0085\ln(P_{L'}/S)}P_{L'}^{-0.07}R_{geo}^{-0.022}\kappa_a^{0.26+0.375\ln(\kappa_a)}F_A^{-0.006+0.0125\ln(F_A)}F_{sh}^{0.04}$$
$$q_{cyl}^{-0.025-0.09\ln(F_A)}(n/n_{Gr})^{0.165-0.1\ln(n/n_{Gr})}\left(P_{L'}/(n^2V)\right)^{0.05\ln\left(P_{L'}/(n^2V)\right)} \quad (3)$$

where $C_{aux} \simeq 1.16$ for standard ITER FEAT operating parameters. This means that the point

Table 4: Weighted averages (a) in engineering units (b) in ITER FEAT units, as well as (c) data variation, $\pm(Q_{0.975}-Q_{0.025})/2$, – *on natural logarithmic scale* – of plasma parameters in the DB4v5 (standard) dataset that has been used to derive Eqs (2) and (3).

	I_pB_t	$P_{L'}$	$P_{L'}/S$	R_{geo}	κ_a	F_A	F_{sh}	q_{cyl}	n/n_{Gr}	$P_{L'}/(n^2V)$	W_{th}[MJ]
(a)	0.648	1.72	-2.29	0.60	0.44	0.083	0.474	0.938	-0.435	24.65	-0.42
(b)	-3.73	-2.76	-0.243	-1.227	0.112	0.132	0.035	0.278	-0.258	4.28	-0.42
(c)	± 1.62	± 1.26	± 1.14	± 0.64	± 0.34	± 1.01	± 0.60	± 0.39	± 0.40	± 4.58	± 2.35

prediction for W_{tot} in ITER (D into D), according to this interaction scaling ('H_{16}(dd,y;tot)'), equals 1.16 × 230 MJ ≃ 265 MJ, which corresponds to $\tau_{E,tot} \simeq 3.0$ s.

As one can see from Eq. (3), at reference operating parameters of ITER FEAT, the quadratic dependence on $P_{L'}/n^2V$ almost disappears ($-0.04 + 0.05 = 0.01$) and both the dependence on (I_pB_t) and on n/n_{Gr} is somewhat stronger (and hence more favourable) when the fast particle fraction W_{fp}/W_{th} is included. Also, the curvature of the κ_a dependence in W_{tot} is different from that in W_{th}, which is (of course) in part related to the presence of κ_a in V. For an early, specific investigation of the κ_a dependence on confinement, the reader is referred to [44, 74]. To keep the regression expressions relatively simple, the interaction between n/n_{Gr} and plasma shape $F_{sh} = q_{95}/q_{cyl}$, see e.g. [55], has *not* been included in Eqs (1) to (3).

Table 5 shows predictions from several (conceptual) machines according to three H–mode and –for comparison– also three L–mode scalings. The multiplication factors for L–mode correspond to the (weighted) average H-factor of W_{th} in the standardised ELMy H–mode dataset that was used to obtain Eqs (2) and (3). In Table 5, MTR (1951) denotes the conceptual device originally proposed in [95], while BPX [27,79] and FIRE [72] are two ignition ('burning plasma') experiments proposed in the USA. The acronym INTOR (1987) [43] stands for a moderately sized, excogitated tokamak ($V = 236$ m^3) with a rather high aspect ratio ($A = R/a = 4.2$), somewhat similar to the ITER-92 ('HARD') device with $A = 4$, the conceptual design of the latter being explicated in [120]. Furthermore, ITER(r) is ITER-03 ('FEAT') operated at reduced reference parameters ($I_p = 12.5$ MA, $\bar{n}_e = 8{\cdot}10^{19}$ m^3, $k_a = 1.4$, $V = 685$ m^3, and, according [33,97,124], at $\delta = 0.4$, $q_{95} = 3.6$) to alleviate somewhat the issue of possible instability against vertical plasma displacements [39, 40, 98] and the severity of ensuing disruptions, see e.g. [36, 47, 81–83, 88, 96, 103]. As has been described in [46, 52, 77] among (many) others, the nominal fusion gain factor $Q = P_{fus}/P_{aux}$, while depending on a number of factors such as helium exhaust, impurity concentration and plasma profile characteristics, is also a sensitive function of τ_E. To provide orientation by a simple estimate, let us keep all other conditions the same as in [52]. Now, from $\tau_{E,th} = 2.5 \times (2.5/2)^{0.2} \times 1.05$ (ITER-03) and $\tau_{E,th} = 2.4 \times (2.5/2)^{0.2} \times 1.1$ (ITER-03(r)) based on Table 5 (applied to D into T, while using multiplication factors 1.05 and 1.1 as rough estimates to obtain optimised

[20] while retaining ALC C–MOD, $W_{fp} = 0$ was used –as an imperfect approximation at present– for ICRH heated discharges

Table 5: Confinement-time prediction (in s) for various tokamak designs (D $\rightarrow$ D plasmas), according to 1.5×L89-P, 1.3×L89-OL and 1.5×L97-P (L–mode), and $H_{98}(y,2)$, H_{16}(dd,y;th) and H_{16}(dd,y;tot) (H–mode) scalings. The last column gives $P_L/P_{L,thresh}$ according formula (4) in [108] while using (for $Z_{\rm eff}=2$) the factor $F(A)^\gamma$ with $F(A)=\frac{0.1A}{1-\sqrt{2/(1+A)}}$, $A=R/a$ and $\gamma=0.5$. For the acronyms of the various devices, see the main text.

device	$1.5\tau_E^{\rm L89\text{-}P}$	$1.3\tau_E^{\rm L89\text{-}OL}$	$1.5\tau_{E,th}^{\rm L97\text{-}P}$	$\tau_{E,th}^{\rm H98(y,2)}$	$\tau_{E,th}^{\rm H16(dd,y)}$	$\tau_{E,tot}^{\rm H16(dd,y)}$	$P_L/P_{L,thresh}$
MTR (1951)	2.02	1.90	3.92	4.00	1.06	1.51	0.3
T-20 (1975)	0.67	0.65	0.51	0.75	0.61	0.80	2.7
BPX (1992) (s)	0.60	0.57	0.55	0.71	0.43	0.48	2.1
BPX (m)	0.90	0.68	0.87	1.07	0.75	0.74	1.2
FIRE (2000)	0.55	0.51	0.75	0.91	0.48	0.62	0.67
INTOR (1987)	0.98	0.83	1.21	1.40	0.98	1.1	1.25
ITER-92 (h)	1.72	1.47	1.74	1.06	0.72	1.14	1.8
ITER-03	2.19	1.74	2.31	3.42	2.5	2.9	1.25
ITER-03 (r)	1.66	1.35	1.57	2.26	2.43	2.87	1.6
JT-60SA	0.37	0.42	0.34	0.44	0.39	0.42	3.0

Table 6: (Weighted) means and ranges ($Q_{0.025}$, $Q_{0.975}$) of H-factors for $\tau_{E,th}$ with respect to L–mode scalings in the DB4v5 ('medium to high density') standard dataset.

scaling	$\tau_E^{\rm L89\text{-}P}$	$\tau_E^{\rm L89\text{-}OL}$	$\tau_{E,th}^{\rm L97\text{-}P}$
DB4v5.std (N=2963)	1.5 (1.04, 2.16)	1.3 (0.70, 2.43)	1.5 (1.03, 2.18)

confinement by prolonged operation at the reduced plasma reference parameters) one gets the estimate $Q\simeq 4$.

One can see from Table 5, for instance, that W_{th} for the very high density and large aspect-ratio circular MTR device from 1951, is rather optimistically (over-)predicted by L97-P and $H_{98}(y,2)$, while the optimisation (with respect to τ_E) of ITER-92(h) device seems more tuned to the L–mode scaling(s) multiplied with an average H–mode factor than to each of the three ELMy H–mode scalings that were developed afterwards.

Besides predicting τ_E in large-scale devices, it is also interesting to see how well the confinement time is predicted in small machines that were constructed and operated well before the database was assembled. To provide an example, two of them, with data taken from [19, 38], are presented in Table 7. (For related additional information on somewhat similar, subsequent tokamak experiments from that era, see e.g. [26,59,91].) While the –somewhat arbitrary– assumption $q_{95}=1.5q_{cyl}$ was made for T–4, downward extrapolation to previous small-machine (ohmic) confinement time seems to be reasonably reliable in this situation.

The scalings in Eqs (1) to (3), which differ mainly for NSTX and (slightly less so) for MAST from H_{06}(dd,y), are to be viewed as a complement to the operational boundaries from Figs 1 and 2. In the absence of more specific experimental information[21] in the database on the sawtooth

[21] other than the simple approximate relations $r_{inv}/a\simeq 1/q_{95}$ and $r_{mix}/a\simeq 1/q_{95}+0.3$ for $2\lesssim q_{95}\lesssim 6$ found at

Table 7: Confinement-time prediction (in s.) in two small-sized (historical) tokamaks (D $\rightarrow$ D plasma), according to L89-P, L89-OL and L97-P (L–mode), and $H_{98}(y,2)$, H_{16}(dd,y;th) and H_{16}(dd,y;tot) (H–mode) scalings.

device	$\tau_E^{\text{L89-P}}$	$\tau_E^{\text{L89-OL}}$	$\tau_{E,th}^{\text{L97-P}}$	$\tau_{E,th}^{\text{H98(y,2)}}$	$\tau_{E,th}^{\text{H16(dd,y)}}$	$\tau_{E,tot}^{\text{H16(dd,y)}}$	$\tau_{E,obs}$	$P_L/P_{L,thresh}$
Pulsator	0.9 %	1.3 %	1.0 %	1.1 %	0.92 %	1.19 %	0.8 %	0.5
T–4	1.0 %	1.1 %	1.1 %	1.0 %	0.8 %	1.6 %	1.6 %	1.2

inversion (or mixing) radius (see e.g. [6,20,34]), as well as on the parameters of the steep gradient zone (see e.g. [114]), where the heat transport mechanisms differ from those in the central confinement region, Eqs (1) to (3) attempt to describe –in a rather elementary way– the overall plasma confinement-time behaviour. Differences in magnetic field ripple among the tokamaks and bearings on plasma rotation (see e.g. [92,102,112]), the latter being partly an engineering and partly a plasma-physics parameter, are interesting, but have not been taken into account. Nevertheless, while specific selection criteria (see [111] and this Annex) have been applied to obtain standardised datasets, these scalings are based on a fairly substantial number of discharges from different devices, and, in the wake of the 2008 IAEA Conference on Fusion Energy held in Geneva [60], they call for a cautionary approach.

Annex 2. (Aspect ratio: availability in H–mode and L–mode)

A particular feature of Eqs (1) and (2) is a rather complicated interaction between aspect ratio, R/a, q_{cyl} and κ_a.[22] It is, therefore, useful to look at the range of 'effective' aspect ratios, $\frac{R_{geo}}{a\sqrt{\kappa_a}}$, that are available in ELMy H–mode 'standard' dataset.

This is shown in Fig. 7, which contains also the positions of several projected (hypothetical) devices (preceded by P_ in the legend): two conventional aspect-ratio machines, ITER FEAT (2003) and T–20 (1975), as well as MTR proposed by Tamm and Sacharov around 1951, presented at the second IAEA conference in Geneva (1958), see [95], and an elongated version of this device, with $\kappa_a = 1.6$, and $(R,a) = (c^{-1}\times 15\,\text{m}, c^{-1}\times 2\,\text{m})$ for $c = 1$ and $c = 2$, respectively, for convenience called MTRe(c)[23] (where e stands for elongated; summary parameters are given in the Appendix). Also in Ref. [78] a case is made for a conceptual tokamak reactor design with a large aspect-ratio, albeit while using a more optimistic assumption about β_N. From Fig. 7, one can see that the database is rather well suited for prediction of conventional aspect-ratio machines, whereas that of large aspect-ratio devices requires a more substantial extrapolation.

The variation of the parameter $f_s = 0.32(R/a)a^{0.25}\kappa^{0.5}$, identified in [122] as a weak principal component (along which merely inaccurate and unreliable extrapolations are possible), has been extended since, mainly by additions from NSTX ($f_s \simeq 0.5$) and START ($f_s \simeq 0.4$) as well as from PBX–M, JT–60U, and TFTR ($1.5 \leq f_s \leq 2.0$). In particular, this dataset (LDB2v10, version

DIII–D, see [104]

[22] At constant minor radius, both S and V depend linearly on R/a.

[23] In line with experience from Alcator C–mod and FTU, see [71,84,85], and unadorned T–20 approach, high magnetic field in MTRe device(s) might be practicable with low temperature (e.g., N_2 or CH_4 – cooled) copper coils, which can have (depending on impurity content) an electrical resistivity about seven times and a thermal resistivity of about a factor 1.5 lower than copper material at room temperature, see e.g. [31,66] and [4, Section D].

as settled around 2007, see [53]) includes large aspect-ratio scans from TFTR and T–10 which were performed in the period 1980 to 2000. From Fig. 5 one can see that here the experimental range in $R/(a\sqrt{k_a})$ comprises the projected (effective) aspect ratio of MTR(e), which indicates a concrete feasibility to produce such type of plasma discharges at least in L–mode.

Summary and Outlook

From the brief comparison in section 1, one may conclude that the more cautious expectation about the confinement time ($\tau_E \sim 1\,\mathrm{s}$), included explicitly by the authors of the T–20 design study, was justified. This value would probably not have been exceeded in practice, neither in L–mode nor in standard ELMy H–mode regime. Secondly, the true performance for inductive ELMy H–mode in the other conceived devices may be less than is often considered required, which could motivate a further enquiry whether or not the above described empirical relations for the upper boundaries $\beta_{N,max}\langle B_p\rangle$ and $n/n_{Gr,max}$ in standard ELMy H–mode and L–mode are of a more fundamental nature. Furthermore, an improvement of the second ELMy H–mode confinement scaling from 1998 (mixed isotope case), as well as two refinements of the interaction scaling from 2006 (for deuterium only), have been given in Annex 1. These scalings describe better the aspect-ratio dependence and are based on essentially the standard deuterium dataset (ITERH.DB4v5, from 2006 IAEA/Chengdu, as frozen February 2007). They call for caution, which was exercised in the original T–20 report, when predicting the plasma stored energy in large-scale future devices. The data has been provided by a number of conventional tokamaks and by two tight aspect-ratio machines. An intriguing problem is the different dependence of W_{th} on q_{cyl} between these (geometrically) different device classes.

The reader is reminded that each of the log non-linear confinement-time scalings, derived in 2006 ('Chengdu'), 2014 ('Eq. 1') and 2016 ('Eqs 2 and 3'), respectively, are based on D into D discharges only. It is recalled that, while most of the available confinement data from the present-day experiments are performed with various admixtures of H and D, large-scale future machines are planned to operate initially in H and He, and, in a later stage, with deuterium and tritium as main isotopes. Further investigation of the precise influence of the isotope mixture (characterised by average atomic mass number M and atomic charge Z) on the confinement time, see e.g. [5, 69], remains therefore an interesting area of further investigation, even though the effect on confinement is notable but not very large. An obvious physical parameter is the (poloidal) gyro-radius, proportional to $\sqrt{M}/Z$ (at constant temperature) and to M/Z (between collisions, for fixed momentum). Also differences in neutral-beam penetration as well as in heat absorption by radio-waves and, consequently, in the electron-ion heat exchange term, P_{ei}, can play a role, whilst the modelling of the various physical processes (to determine W_{th} based on W_{mhd}, W_{dia}, and W_{fp}, occasionally validated against (electron and ion) temperature and density profile data), is quite intricate, see e.g. [15, 62, 90, 101], while foundational issues [18, 24] –often more controversial than concrete applications– leave room for further enquiry.

As can be viewed from Figs 6 and 7, the distribution of the pure isotope discharges (i.e., H into H and D into D) currently available in the L–mode confinement DB ('LDB.2v10') appears to be rather scant to derive separate isotope confinement-time scalings in a reliable manner, and, in particular, to investigate the question whether the difference in q_{cyl} dependence of τ_E between low and high aspect-ratio plasmas also pertains to L–mode. In this context, it may be useful to recall that a considerable variation of τ_E with q_{cyl} for various conventional tokamaks has already been described in [122], where it was expressed as a multiplication factor $(q_{cyl}/3.2)^{f_q}$ with $|f_q| < 0.2$, and was based on the mixed isotope dataset that was afterwards called LDB.1. In principle,

L–mode plasmas seem to be rather suitable for a further investigation of this issue, since their intrinsic heat transport is not influenced by ELMs. Revisiting the topic of plasma confinement scaling also in L–mode would not change the significance of the remark from the preliminary T–20 design study cited in the first section of this report.

Acknowledgments

The title of this report is slightly deceptive, since the last part presents an analysis of confinement data that have been assembled during the period 1982-2006, i.e., well after the initial T–20 design study. As is apparent from the references as well, this was an international effort made possible by both institutional and individual researchers' engagement, and focused by ITER expert group meetings. The title has been left unchanged as a tribute to the pioneering work in this area at Kurchatov Institute. Specifically, the author wishes to acknowledge V.S. Mukhovatov for drawing attention – during a discussion at the ITPA meeting in Lausanne, Spring 2007 – to the existence of translated version of the T–20 Design Study, and Dr. A.C. Chudnovskiy for several dry and useful subsequent remarks. Dr. P.T. Lang is acknowledged for stressing importance of the high density regime, which led to the scalings in this report being based on medium to high densities, and Dr. G. Pautasso for suggesting (initial) operation of ITER FEAT at reduced parameters. Finally, the author wishes to express his gratitude to Prof. Dr. F. Wagner for expressing general interest, as well as to Dr. F. Herrnegger for some close reading, helicopter-view discussions, and organising invaluable tea-time conversations with W7-AS marksmen.

Appendix

Parameters of MTR (left, 1951) and T–20 (right, 1975) devices

a.) geometrical (pertaining to the plasma itself)

Rgeo = 12 m — major radius — 5 m

amin = 2 m — minor radius — 2 m

kappa = 1 — elongation (limiter only) — 1

S = 960 m^2 — surface area — 400 m^2

V = 960 m^3 — volume — 400 m^3

b.) plasma current, magnetic field on axis and (reference) plasma density:

$|I_p| = 5$ MA — current — 6 MA

$|B_t| = 5$ T — toroidal magnetic field — 3.5 T

$q_{cyl} = (5/3)$ — safety factor — (7/3)

$\bar{n}_e = 3 \times 10^{20}\,\mathrm{m}^{-3}$ — plasma density — $5 \times 10^{19}\,\mathrm{m}^{-3}$

c.) expected ('predicted') values T–20 (as of 1975):

$T_e = 3$ keV — (average) plasma temperature (ohmic heating)

$T_e = 10$ keV (possibly: 5 keV) — (average) plasma temperature (with auxiliary heating)

$\tau_E = 2\,\mathrm{s}$ (possibly: 1 s) — energy confinement time

$W_{th} = 100$ MJ (possibly: 50 MJ) — stored plasma energy

$\beta_p \simeq 1$ (possibly: $\beta_p \simeq 0.5$) — poloidal beta

$P_{L'} = W_{th}/\tau_E = 50$ MW — power transfer ('loss') across the last closed flux surface

$P_w = P_{L'}/S = (1/8)$ MW/m^2 (possibly: $\simeq (1/4)$ MW/m^2) — averaged wall heat load

Parameters of ITER FEAT (left, 2003) and MTRe(c) (right, hypothetical) devices

a.) geometrical (pertaining to the plasma itself):

Rgeo = 6.2 m — major radius — $c^{-1} \times 15$ m

amin = 2 m — minor radius — $c^{-1} \times 2$ m

$\kappa_a = 1.6$ — elongation (divertor)— 1.6

S = 680 m^2 — surface area — $c^{-2} \times 1570$ m^2

V = 830 m^3 — volume — $c^{-3} \times 1920$ m^3

b.) plasma current, magnetic field on axis and (reference) plasma density:

$|I_p| = 15$ MA — (absolute) current — $c^{-1} \times 10$ MA

$|B_t| = 5.3$ T — (absolute) toroidal magnetic field — 10 T

$q_{cyl} = 1.82$ — safety factor $(= 5\frac{B_t}{I_p}\frac{a^2\kappa_a}{Rgeo})$ — 2.13

$\bar{n}_e = 1 \times 10^{20}$ m^{-3} — plasma density — $c \times 6 \cdot 10^{19}$ m^{-3}

c.) power across LCFS, 'magnetic design', and 'dimensionless' parameters (projected, $c = 1$):

$P_{L'} = 87.7$ MW — W_{th}/τ_E — 150 MW

$P_{L'}/S = 0.128$ MW/m^2 — averaged wall heat load — 0.096 MW/m^2

$\langle B_p \rangle = 1.1\,\mathrm{MA/m}$ — $\mu_0 I_p/L$ — $0.75\,\mathrm{MA/m}$

$\beta_N \frac{\langle B_p \rangle}{1.2} = 1.5\,\mathrm{MA/m}$ — (see Table 3 & Figs 1 and 2) — $0.7\,\mathrm{MA/m}$.

$n/n_{Gr} = 0.838\,\mathrm{m^{-1}MA^{-1}}$ — $\frac{\bar{n}_e}{I_p/\pi a^2}$ — $0.76\,\mathrm{m^{-1}MA^{-1}}$

$\beta_t[\%] = 2.3$ — $2\mu_0[(2/3)W_{th}]/(\langle B_t \rangle^2 V)$ — 0.55

$\beta_N = 1.63$ — $100(aB_t/I_p[\mathrm{MA}])\beta_t$ — 1.1

$\rho_{*,p,ion} = r_{*,p,ion}/(L/2\pi) \approx 0.9\%$ — $\sim (\sqrt{M_{\mathrm{eff}}}/Z)(\sqrt{\langle T \rangle}/I_p)$ — $\approx 1.7\%$

Relative weights used for regression

In order to account approximately for the imbalance of the number of discharges per tokamak contributed, the following weights have been used to derive the scaling expressions in this report, according to a rounded version of the inverse weight function $2 + \frac{\sqrt{N_j}}{4}$, as described in [13, 55].

Table 8: Relative tokamak weights applied for least-squares regression in this text; fdr: full density range, rdr: restricted density range, both based on standard selection criteria to obtain standard subset of DB4v5. The weights rdr have been used to derive Eqs (2) and (3).

	asd	aug	cmo	com	d3d	jet	jft	jt6	mas	nst	pbx	pdx	t10	tde	tft
Eq. (1)	3/2	1/2	1	4/3	2/3	1/3	1	1	1	2/3	1	1	3	3	3/2
Eq. (2-3) fdr	1	2/5	1	4/3	2/3	1/3	1	1	1	4/5	1	1	4/3	4/3	3/2
Eq. (2-3) rdr	4/3	2/5	1	-	2/3	4/11	1	1	1	4/5	4/3	1	-	2	4/3

References

[1] Alikaev, V.V., Glukhikh, V.A., Dnestrovskij, Y.N., Ivanov, D.P. et al., *Experimental Thermonuclear Installation* – TOKAMAK–20 – *Preliminary Study, Vol II, part 2, Enginering Solutions*, National Committee for the Utilization of Atomic Energy, Soviet Ministry, USSR. I.V. Kurchatov Atomic Energy Institute, D.V. Yefremev Scientific Research Institute for Electrophysical Apparatus, Moscow, 1975. Translated by Igor N. Sviatoslavsky, University of Wisconsin Fusion Design Study Group, Report UWFDM-129.

[2] Alonso, M. and Finn, E.J., *Fundamental University Physics*, Vol. II, Addison-Wesley, Reading, Massachusetts, second edition, 1983. (First edition: 1967)

[3] Artsimovich L.A. et al., Plasma Physics and Controlled Nuclear Fusion Research (Proc. 4th Int. Conf., Madison 1971), Vol. 2, IAEA, Vienna (1971) 443.

[4] Becker, R., *Theorie der Elektrizität*, dritter Band: *Elektrodynamik der Materie.* Herausgegeben und verfaßt von F. Sauter, Teubner–Verlag, Stuttgart, 1968.

[5] Bessenrodt–Weberpals, M. et al., Nuclear Fusion **33** (1993) 1205–1238.

[6] Biskamp, D., *Nonlinear Magnetohydrodynamics*, Ch. 8.1, Cambridge University Press, Cambridge, United Kingdom, 1993.

[7] Borrass, K., Schneider, R. and Farengo, R., Nuclear Fusion **37** (1997) 523–537.

[8] Challis, C.D., Garcia, J. et al., Improved confinement in JET high β plasmas with an ITER-like wall, Nuclear Fusion **55** (2015) 053031 (18 pp).

[9] Chen, F.F., *Introduction to Plasma Physics and Controlled Fusion*, Plenum Press, New York, second edition, 1984. (First edition: 1974, Third edition: Springer, 2016)

[10] Chen, D.-G., Lin, F., Chen, X., Rang, W., Kitzman, H. Nurs. Res. **63** (2014) 211–220.

[11] Christiansen, J.P., Cordey, J.G., Kardaun, O. and Thomsen, K., Nuclear Fusion **31** (1991) 2127–2129.

[12] Christiansen, J.P., DeBoo, J., Kardaun, O., Kaye, S.M., Miura, Y. et al., Nuclear Fusion **32** (1992) 291–338. Corrigenda **32** (1992) 1281 and **48** (2008) 099801.

[13] Cordey, J.G., Thomsen K., Chudnovskiy, A. et al., Nuclear Fusion **45** (2005) 1078–1084.

[14] DeVries, P.C., Johnson, M.F., Segui, I. and JET EFDA Contributors, Nuclear Fusion **49** (2009) 055011 (12 pp).

[15] Drenik, A., Alegre, D., Brezinsek, S. et al., Physica Scripta **T170** (2017) 014021 (7 pp).

[16] Duan, X.R., Dong, J.Q., Yan, L.W., Ding, D.W. et al., Nuclear Fusion **50** (2010) 095011 (7 pp).

[17] Duan, X.R., Liu, Y., Xu, M., Yan, L.W. et al., Nuclear Fusion **57** (2017) 102013 (11 pp).

[18] Engelhardt, W., Physics Essays **18** (2005) 504–513.

[19] Engelhardt, W., Klüber, O., Meisel, D., Murmann, H., Sesnic, S. et al., Proc. 7th Conf. Plasma Physics and Controlled Fusion Research, Innsbruck 1978, Vol. I, 123–134, Vienna 1979, IAEA-CN-37/A-5.

[20] Engelmann, F., Plasma Physics Control. Fusion **32** (1990) 1101–1113.

[21] Engen, S., *Stochastic Abundance Models,* Monographs on Statistics and Applied Probability, Chapman and Hall, London, 1978. (Reprinted by Springer Netherlands)

[22] Fukuda, T., Takizuka, T., Tsuchiya, K., Kamada, Y. et al., Nuclear Fusion, **37** (1997) 1199–1213.

[23] Glasstone, S. and Lovberg, R.H., *Controlled Thermonuclear Reactions*, Van Nostrand Reinhold, 1960. (German translation: Einführung in die theoretische und experimentelle Plasmaphysik, Karl Thiemig KG, München, 1964.)

[24] Goedbloed, J.P., Plasma Physics Control. Fusion **60** (2018) 014001 (5 pp).

[25] Goldstein, H., Classical Mechanics, second edition, Addison-Wesley, 1980. (First edition: 1950)

[26] Goldston, R.J., Plasma Physics Control. Fusion **26** (1984) 87–103.

[27] Goldston, R.J., Fusion Technology **21** (1992) 1050–1055.

[28] Grasman, R.P.P.P., Van der Maas, H.L.J., and Wagenmakers, E.-J., Jounal of Statistical Software **32** (2010), Issue 8, available on internet, URL = http://jstatsoft.org/

[29] Greenwald, M., Plasma Physics Control. Fusion **44** (2002) R27–R80.

[30] Greenwald, M., Terry, J.L., Wolfe, S.M., Ejima, S., Bell, M.G., Kaye, S.M., Neilson, G.H., Nuclear Fusion **28** (1988) 2199–2207.

[31] Gray, D.E., Coordinating Editor, *American Institute of Physics Handbook*, third edition, McGraw-Hill, 1972. (First edition: 1957)

[32] Gruber, O. for the ASDEX Upgrade Team, Nuclear Fusion **47** (2007) S622–S634.

[33] Gruber, O., Fusion Engineering and Design, **84** (2009) 170–177.

[34] Gude, A., Maraschek, M., Kardaun, O., and the ASDEX Upgrade Team, Plasma Physics Control. Fusion **59** (2017) 095009 (14 pp).

[35] Günter, S. et al., Nuclear Fusion **45** (2005) S98–S108.

[36] Hender, T.C., Wesley, J.C. et al., ITER Physics Basis Progress, Chapter 3, Nuclear Fusion **47** (2007) S128–S202.

[37] Huba, J.D., NRL Plasma Formulary (2013), Naval Research Laboratory, Washington, DC 20375.

[38] Hugill, J. and Sheffield, J., Nuclear Fusion **18** (1978) 15–22.

[39] Humpreys, D.A. et al., Nuclear Fusion **49** (2009) 115003 (10 pp).

[40] Humpreys, D.A. et al., Plasma Control Studies Using DIII–D Design Tools in Support of ITER, 26^{th} IAEA Fusion Energy Conference, Kyoto 2016, EXS/P6-37 (8p, in preparation for publication).

[41] Insightful Corporation, 2007, *S-Plus 8.0 Guide to Statistics*, Vol. 2, Seattle, WA, USA.

[42] Ishida, S., Barabaschi, P., Kamada Y. and the JT–60SA Team, Nuclear Fusion **51** (2011) 094018 (12 pp).

[43] INTOR Group, *International Tokamak Reactor, Phase One*, IAEA, Vienna, 1982, STIO / PUB / 619, ISBN 92-0-131082-X and *Phase Two A, Part III*, IAEA, Vienna, 1988, STIO / PUB / 795, ISBN 92-0-131188-5.

[44] ITER Expert Groups and ITER Physics Basis Editors, Nuclear Fusion **39** (1999) 2137–2664.

[45] JT–60SA Research Unit, JT–60SA Research Plan –research objectives and strategy– version 3.3, March 2016, available on internet, URL = http://jt60sa.org/pdfs/JT-60SA/JT-60SA_Res_Plan.pdf

[46] Johner, J., Fusion Science and Technology **59** (2011) 308–331.

[47] Kadomtsev, B.B., Plasma Physics Control. Fusion **26** (1984) 217–226.

[48] Kamada, Y., Isayama, A., Oikawa, T., Sakamoto, Y. et al., Nuclear Fusion **39** (1999) 1845–1853.

[49] Kamada, Y., Barabaschi, P., Ishida, S., the JT–60SA Team and JT–60SA Research Plan Contributors, Progress of the JT–60SA Project, 24th IAEA Fusion Energy Conference, San Diego 2012, OV/4-1.

[50] Kardaun, O., Kus, A., H– and L–mode Database Working Group, in Prat, A. (Editor): Computational Statistics XII (Proc. 12^{th} Symposium on Computational Statistics, Barcelona, 1996), 313-318, Physica-Verlag, Heidelberg.

[51] Kardaun, O., Kardaun, J., Itoh, S.-I. and Itoh, K., in: Controlled Fusion and Plasma Physics (Proc. 25th EPS Conference on Control. Fusion and Plasma Physics, Prague, 1998), volume 22C, 1975-1978.

[52] Kardaun, O., Nuclear Fusion **42** (2003) 841–852.

[53] Kardaun, O. et al., Synopsis (IAEA 2006, Chengdu) — Revised Version 3: February 2007 (IT/P1-10) 1–2, available on internet URL = http://www2.ipp.mpg.de/~Otto.Kardaun/-rep.html

[54] Kardaun, O. for the H–mode DB WG, Proc. 14th Conf. Plasma Physics and Controlled Fusion Research, Würzburg 1992, 3: 251–270, 1993, IAEA-CN-56/F-1-3.

[55] Kardaun, O., Report IPP-IR-2002/5-1.1, MPI für Plasmaphysik, Garching bei München, available on internet, URL = http://www2.ipp.mpg.de/~Otto.Kardaun/netreports/ipp/index.html

[56] Kardaun, O., *Classical Methods of Statistics* (with Applications in fusion-oriented Plasma Physics), Springer-Verlag, Heidelberg, 2005.

[57] Kaye, S.M., Gerhardt, S., Guttenfelder, W., Maingi, R. et al., Nuclear Fusion **53** (2013) 063005 (8 pp).

[58] Kaye, S.M., ITER confinement DB WG, Nuclear Fusion **37** (1997) 1303–1328.

[59] Keilhacker, M. et al., Plasma Physics Control, Fusion **26** (1984) 49–63.

[60] Kikuchi, M., Nuclear Fusion **50** (2010) 010202 (1pp) - Editorial.

[61] Koch, K-R., *Parameterschätzung und Hypothesentests in linearen Modellen,* Ferdinand Dümmler Verlag, Bonn, 2. Auflage, 1987.

[62] Kurzan, B., Jakobi, M., Murmann, H. and the ASDEX Upgrade Team, Plasma Physics Control. Fusion **46** (2004) 299–317.

[63] Landau, L.D. and Lifschitz, E.M., Статистическая Физика Теория Поля, NAUKA, Moscow, seventh edition, 1988. (German edition: Klassische Feldtheorie, Harri Deutsch Verlag, Frankfurt am Main, 12. Auflage, 1992, 2009.)

[64] Lang, P.T. et al., Pellet-induced high-density phases during ELM suppression in ASDEX Upgrade, 24^{th} IAEA Fusion Energy Conference, San Diego 2012, EX/P4-01 (8 p).

[65] Lang, P.T., Suttrop, W. et al., Nuclear Fusion **52** (2012) 023017 (11 pp).

[66] Lide, D.R., Editor-in-Chief, *CRC Handbook of Chemistry and Physics*, 83^{rd} edition, CRC Publishing Company, 2003. (First edition: 1913, 98^{st} edition (Editor-in-Chief J.R. Rumble): 2017)

[67] Lloyd, B. et al., Nuclear Fusion **51** (2011) 094013 (10 pp).

[68] Luce, T.C., Humpreys, D.A., Jackson, G.L. and Solomon, W.M., Nuclear Fusion **54** (2014) 093005 (12 pp).

[69] Maggi, C.F., Weisen, H., Hillesheim, J.C., Chankin, A. et al., in: Controlled Fusion and Plasma Physics (Proc. 44th EPS Conference on Control. Fusion and Plasma Physics, Belfast, 2017), volume 41F, I5.013.

[70] Maraschek, M. et al., Nuclear Fusion **45** (2005) 1369–1376.

[71] Marmar, E.S. et al., Nuclear Fusion **55** (2015) 104020 (22 pp).

[72] Meade, D.M. et al., *Mission and Design of the Fusion Ignition Research Experiment (FIRE)*, IAEA-CN-77-FTP2/16, 18^{th} Fusion Energy Conference (2000) Sorrento.

[73] Mirnov, S.V., Plasma Physics and Controlled Nuclear Fusion Research (Proc. 9th Int. Conf., Innsbruck 1978), Vol. 1, IAEA, Vienna (1979) 433–441.

[74] Miura, Y., Takizuka, T., Tamai, H., Matsuda, T. et al., Nuclear Fusion **32** (1992) 1473–1479.

[75] Mukhovatov, V.S., *Tokamaks.* Short contribution ([26-86-4]) in: Great Soviet Encyclopedia, Vol. 26, paper version (a translation of the third edition), McMillan Inc., New York (1981). Russian original: A.M. Prokhorov, Editor in Chief, Болшая Советская Енциклопедя, Publishing House, Moscow (1977).

[76] Mukhovatov, V.S. and Houlberg, W. (Editors), ITER Physics Guidelines, Version 1.0 (October 2007). Report from the Nominee Director-General to Scientific and Technical Advisory Committee, November 2007 (available on request).

[77] Mukhovatov, V.S., Shimada, M., Lackner, K., Campbell, D., Uckan, N.A., Wesley, J.C. et al., ITER Physics Basis Progress, Chapter 9, Nuclear Fusion **47** (2007) S404–S413.

[78] Murakami, Y., Shinya, K., and Nishio, S., Fusion Engineering and Design, **48** (2000) 347–354.

[79] Neilson, G.H. Jr., Fusion Technology **21** (1992) 1056–1075.

[80] Ninomiya, H. and the JT–60 Team, Physics of Fluids B **4** (1992) 2070.

[81] Pautasso, G., Coster, D., Eich, T., Fuchs, J.C. et al., Plasma Physics Control. Fusion **51** (2009) 124056 (11 pp).

[82] Pautasso, G., Zhang, Y., Reiter, B. et al., Nuclear Fusion **51** (2011) 103009 (9 pp).

[83] Pautasso, G., Bernert, M., Dibon, M., Duval, B. et al., Plasma Physics Control. Fusion **59** (2017) 014046 (11 pp).

[84] Pieroni L. et al., Nuclear Fusion **30** (1990) 1957–1960.

[85] Pucella, G. et al., Nuclear Fusion **55** (2015) 104005 (11 pp).

[86] Pucella, G., D'Arcangelo, O., Tudisco, O., et al. Plasma Physics Control. Fusion **59** (2017) 085011 (7 pp).

[87] Pulsator Team, Nuclear Fusion **25** (1985) 1059–1063.

[88] Pustovitov, V.D., Rubinacci, G. and Villone, F., Nuclear Fusion, **57** (2017) 126038 (10 pp).

[89] Rao, C.R., Journal of the American Statistical Association, **65** (March, 1970) 161–172.

[90] Rathgeber, S.K., Fischer, R., Fietz, S. et al., Plasma Physics Control. Fusion, **52** (2010) 095008 (16 pp).

[91] Razumova, K.A., Plasma Physics Control, Fusion **26** (1984) 37–47.

[92] Rice, J.E., Plasma Physics Control. Fusion **58** (2016) 083001 (18 pp).

[93] Ryter, F., H–mode Database Working Group, Nuclear Fusion **36** (1996) 1217–1264.

[94] SAS Institute Inc, 2014, SAS/STAT 9.4 User's Guide, Cary, NC, USA.

[95] Sacharov, A.D., *Theory of a magnetic thermonuclear reactor* (*Part II*), in: Plasma Physics and the Problem of Controlled Thermonuclear Reactions, Vol. I, M.A. Leontovich, Editor, Translated from the Russian by A.R. Hochstim, Translation Editor: H. Motz (Oxford University), Pergamon Press, 1961. Физика плазмы и проблема управляемых термоядерных реакции, том 1, издательство академии наук СССР, 1958.

[96] Schüller, F.C., Plasma Physics Control. Fusion **37** (1995) A135–A162.

[97] Schweinzer, J., Sips, A.C.C., Tardini, G., Schneider, P.A. et al., Nuclear Fusion **51** (2011) 113003 (7 pp).

[98] Sehmer, T., Lackner, K., Strumberger, E. et al., Fusion Science and Technology, **70** (2016) 73–82.

[99] Serfling, R.J., *Approximation Theorems of Mathematical Statistics*, Wiley, New York, first edition, 1980. Reprinted 2001.

[100] Shirai, H., Barabaschi, P., Kamada, Y. and the JT–60SA Team, Nuclear Fusion **57** (2017) 102002 (14 pp).

[101] Schneider, P.A., Bustos, A., Hennequin, P., Ryter, F. et al., Nuclear Fusion **59** (2017) 066003 (15 pp).

[102] Shinohara, K., Kawashima, H., Tsuzuki, K., Urata, K. et al., Nuclear Fusion, **43** (2003) 586–593.

[103] Smith, H.M., Fehér, T., Fülöp, T., Gál, K. and Verwichte, E., Plasma Physics Control. Fusion, **51** (2009) 124008 (8 pp).

[104] Snider, R.T., Nuclear Fusion **30** (1990) 2400–2405.

[105] Stacey, W.M., Nuclear Fusion **47** (2007) 217–221.

[106] Stam, A.J., Statistica Neerlandica **41** (1987) 151–173.

[107] Stäbler, A., Sips, A.C.C. et al., Nuclear Fusion **45** (2005) 617–625.

[108] Takizuka, T., Plasma Physics Control. Fusion **46** (2004) A227-A233.

[109] Takizuka, T., Plasma Physics Control. Fusion **40** (1998) 851–855.

[110] Thomsen, K. et al., *International H–mode confinement database*, available on internet, URL = http://efdasql.ipp.mpg.de/igd/.

[111] Thomsen, K., Kardaun, O., DeBoo, J., Miura, Y., Kaye, S.M. et al., Nuclear Fusion **34** (1994) 131-167.

[112] Tobita, K., Tani, K., Kusama, Y., Nishitani, T. et al., Nuclear Fusion, **35** (1995) 1585–1591.

[113] Troyon, F., Gruber, R., Sauremann, H., Semenzato, S. and Succi, S., Plasma Physics Control. Fusion **26** (1984) 209–215.

[114] Urano, H., Nuclear Fusion **54** (2014) 116001 (15 pp).

[115] Valovič, M. et al., Nuclear Fusion **49** (2009) 075016 (8 pp).

[116] Van der Genugten, B.B., Statistica Neerlandica **47** (1993) 111–125.

[117] Vershkov, V.A., Sarychev, D.V., Notkin, G.E., Shelukhin, D.A. et al., Nuclear Fusion **57** (2017) 102017 (15 pp).

[118] Wagner, F. et al., Physical Review Letters **49** (1982) 1408–1412.

[119] Wesley, J.C. et al., Fusion Technology **32** (1997) 495–525.

[120] Wesley, J.C. and the U.S. ITER Home Team, Fusion Technology **21** (1992) 1380–1388.

[121] Yang, Q.W., Liu, Y., Ding, X.T., Dong, J.Q. et al., Nuclear Fusion **47** (2007) S635–S644.

[122] Yushmanov, P.N., Takizuka, T., Riedel, K.S., Kardaun, O. et al., Nuclear Fusion **30** (1990) 1999–2008.

[123] Zohm, H., et al., Plasma Physics Control. Fusion **45** (2003) A163–A173.

[124] Zohm, H. for the ASDEX Upgrade Team and the EUROfusion MST1 Team, Nuclear Fusion **55** (2015) 104010 (12 pp), Section 7.1.

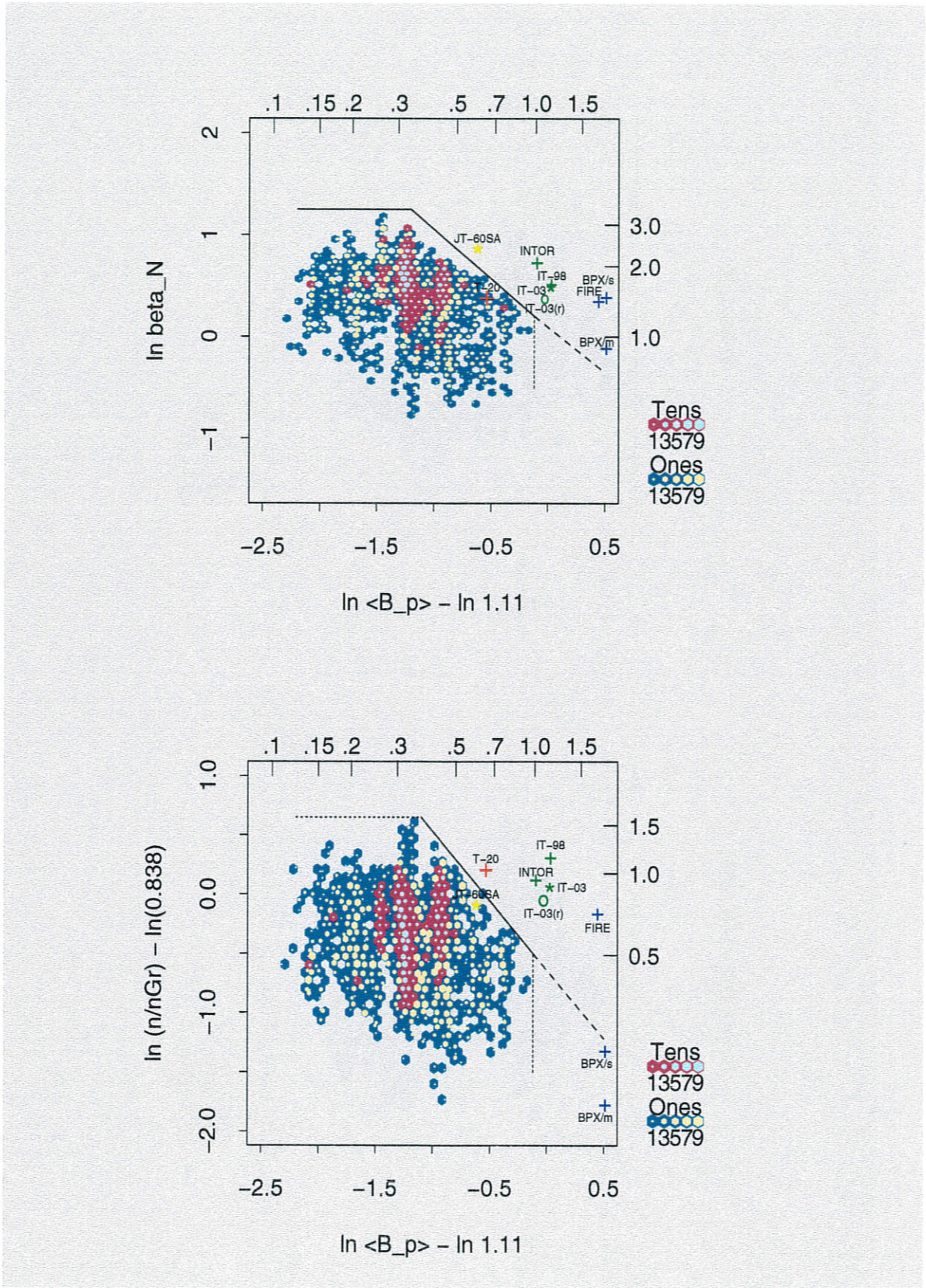

Figure 1: ELMy H–mode data set (see text) and several projected devices. (A) Normalised toroidal β as observed; *for envisaged devices as predicted by* $H_{98}(y,2)$ H–mode scaling, versus the averaged poloidal magnetic field $\langle B_p \rangle = \mu_0 I_p / L$ divided by 1.11, (B) plasma density $\bar{n}_e$ normalised by 0.838 times the Greenwald limit $n_{Gr} = I_p/(\pi a^2)$ versus $\langle B_p \rangle / 1.11$. The data are plotted on a logarithmic scale. The upper horizontal axis displays $\langle B_p \rangle$[MA/m] and the left vertical axis $n/n_{Gr}[10^{20}\,\mathrm{MA^{-1}m^{-1}}]$.

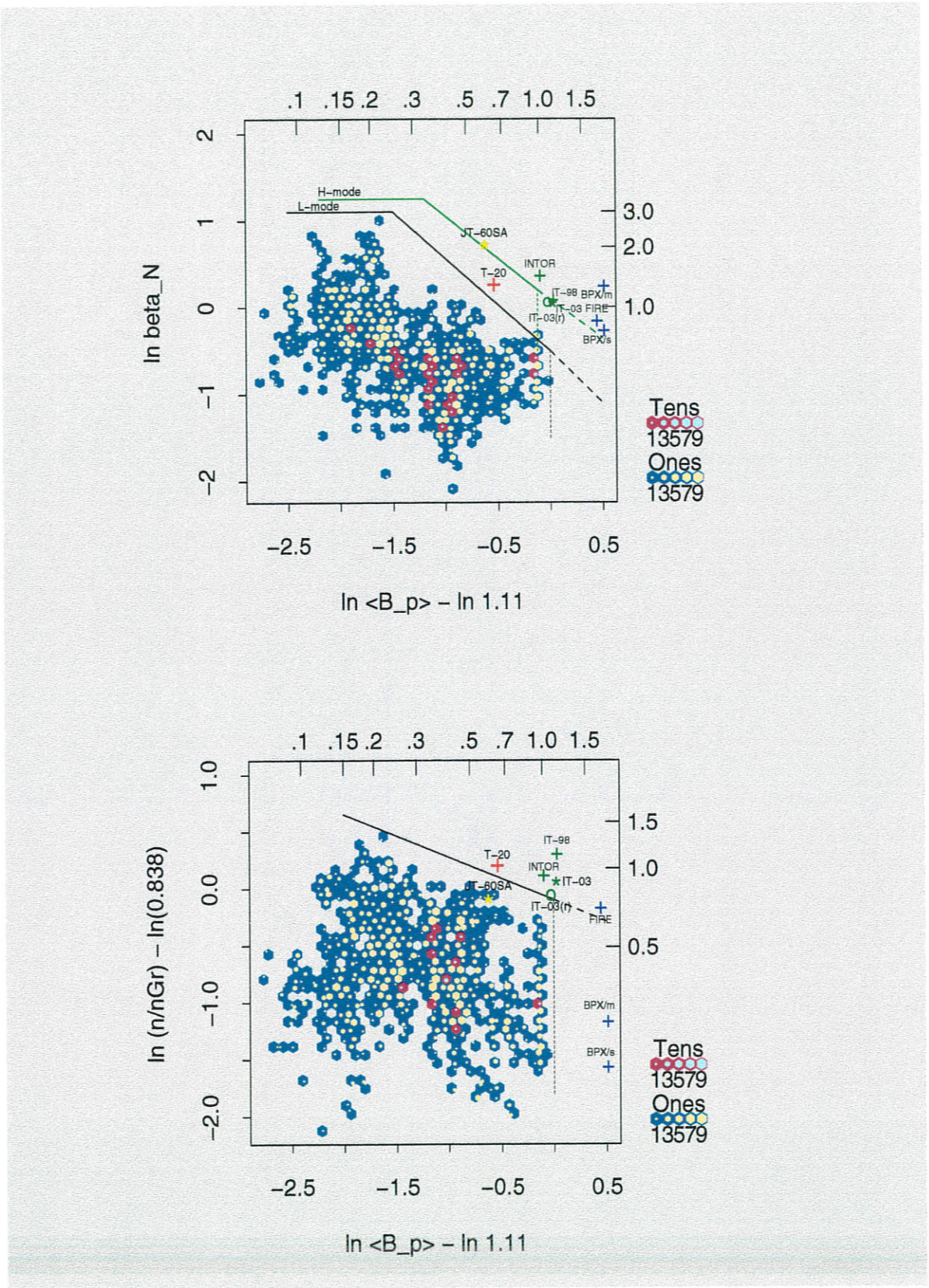

Figure 2: L–mode data set (see text) and several envisaged devices. (A) Normalised toroidal β as observed; *for projected devices, as predicted by* 1.5× L89-P L–mode scaling versus the averaged poloidal magnetic field $\langle B_p \rangle = \mu_0 I_p / L$ divided by 1.11, (B) plasma density normalised by 0.838 times the Greenwald limit $n_{Gr} = I_p/(\pi a^2)$ versus $\langle B_p \rangle$. The data are plotted on a logarithmic scale. The upper horizontal axis displays $\langle B_p \rangle$[MA/m] and the left vertical axis $n/n_{Gr}[10^{20}\,\mathrm{MA^{-1}m^{-1}}]$.

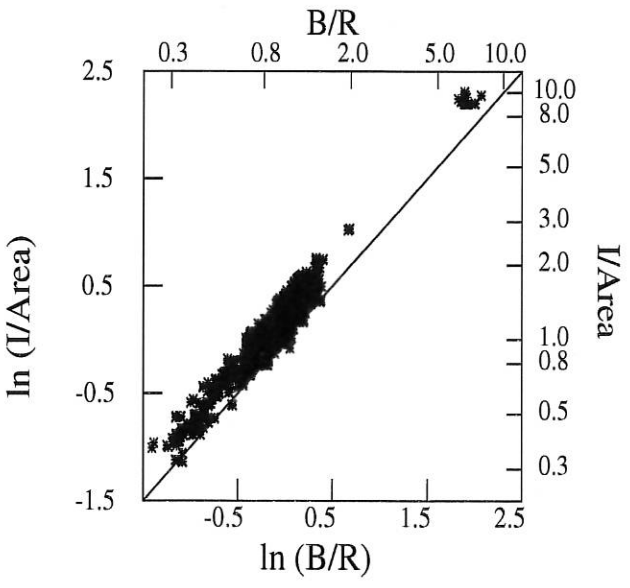

Figure 3: *ELMy H–mode data of conventional aspect-ratio tokamaks.* Plasma current density $I_p/(a^2\kappa_a)$ versus B_t/R. The ratio is $q_{cyl} = 5(B_t/I_p)(a^2\kappa_a/R)$ on a logarithmic scale. The origin corresponds to ITER FEAT. A high current density is favourable to operate at a high plasma density. A high value of B_t/R corresponds to a relatively compact device. The existing gap between AUG/JET/TdeV and ALC C–mod indicates possible room for a further technico-physical experiment.

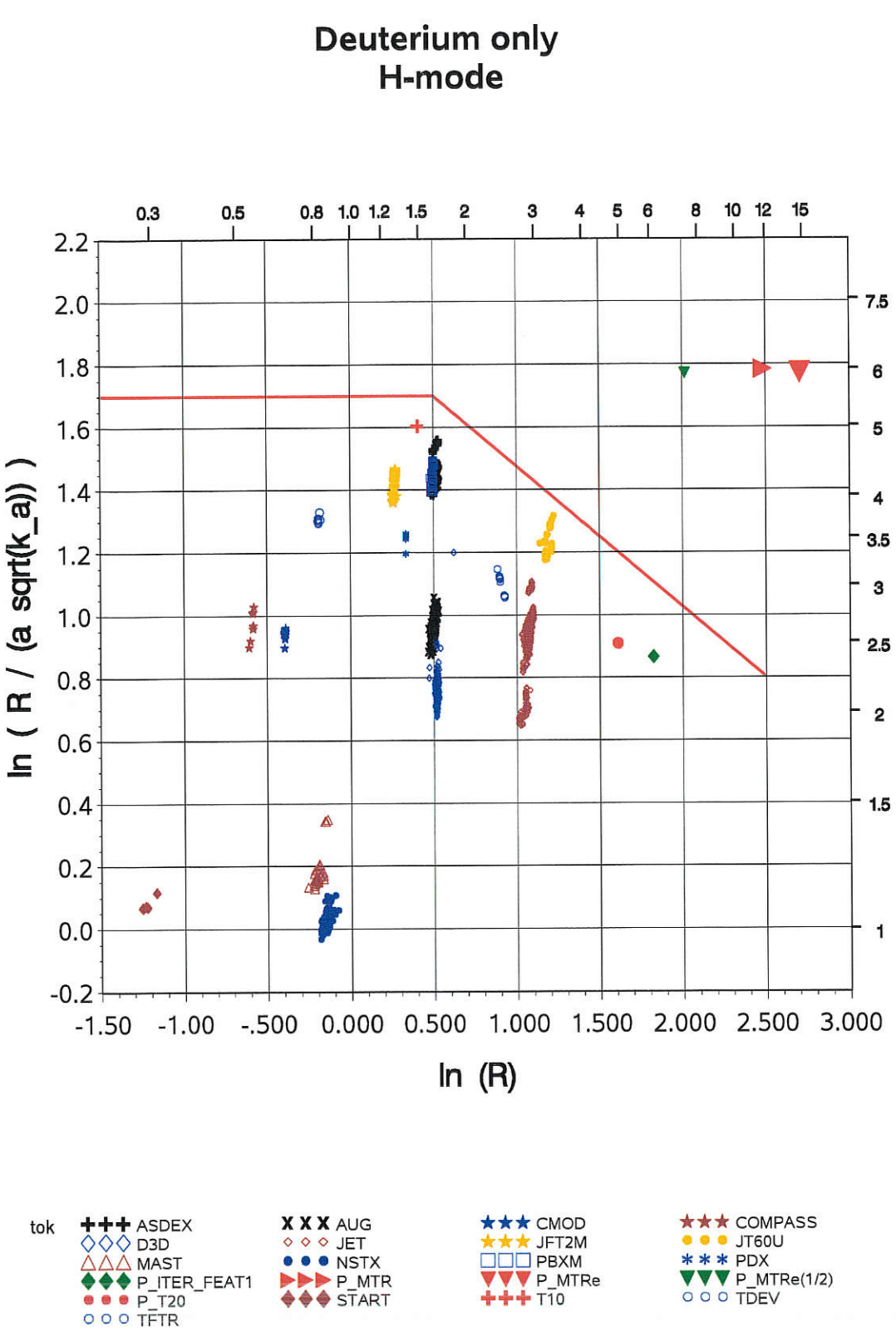

Figure 4: *H–mode data.* Effective aspect ratio, $\frac{R_{geo}}{a\sqrt{\kappa_a}}$, against R_{geo} for the standard confinement dataset (D into D), as well as for several projected devices (with $\ln(R_{geo}) > 1.5$): ITER FEAT, T–20, and MTR(e; c=1, c=2).

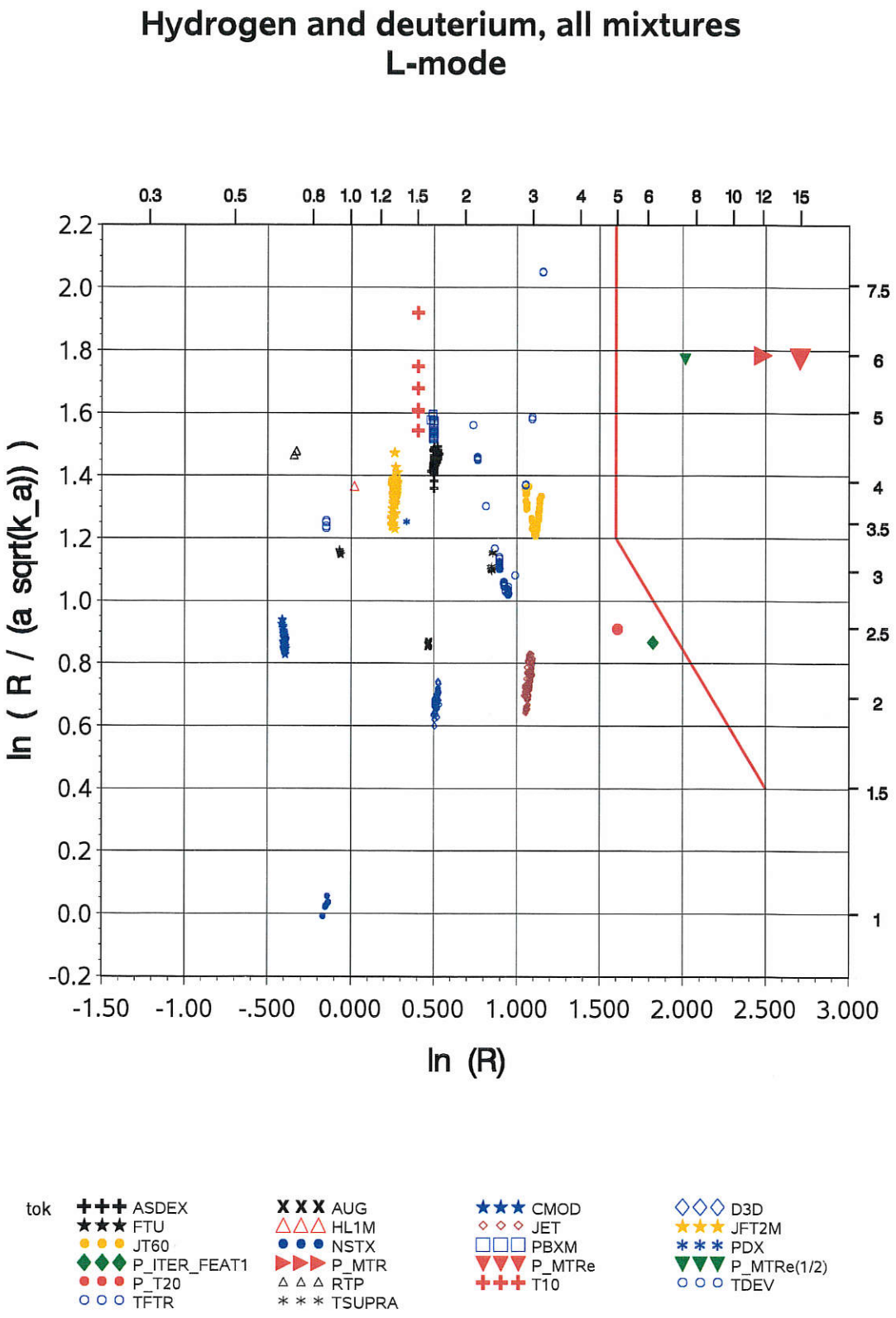

Figure 5: *L–mode data.* Otherwise same legend as in Fig. 4.

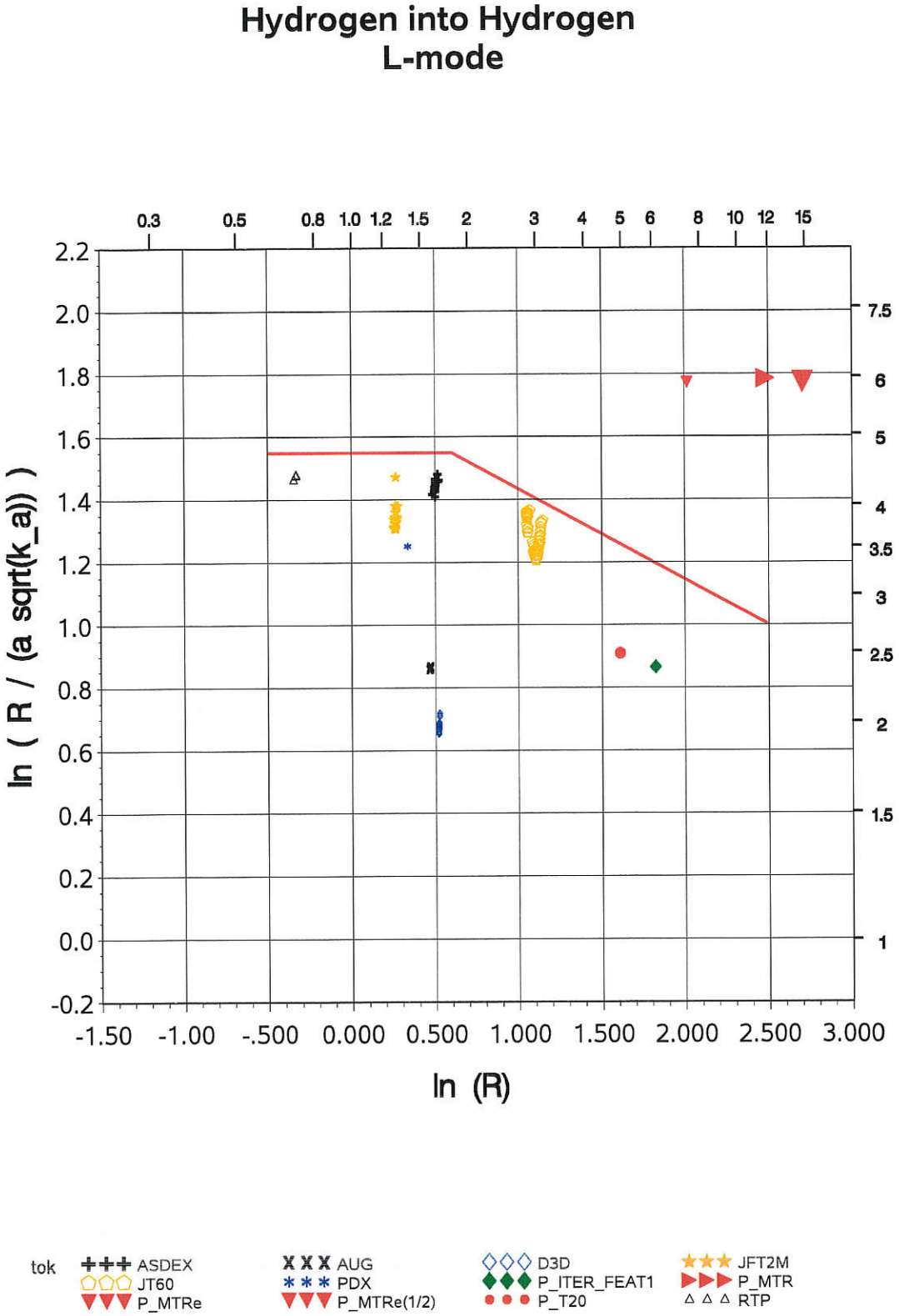

Figure 6: *L–mode data.* DB2v10, standard subset (H → H), otherwise same legend as in Fig. 4.

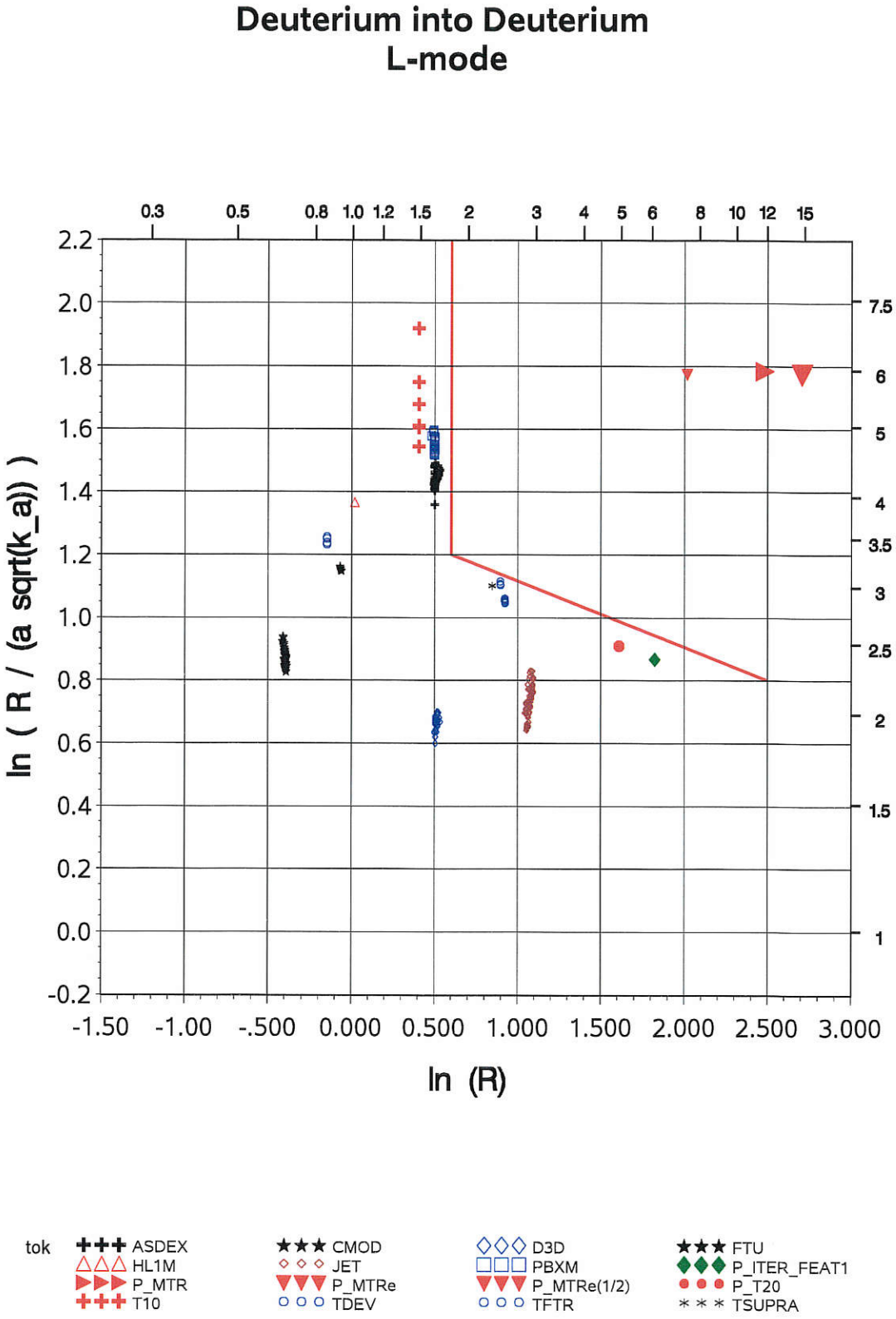

Figure 7: *L–mode data.* DB2v10, standard subset (D → D), otherwise same legend as in Fig. 4.

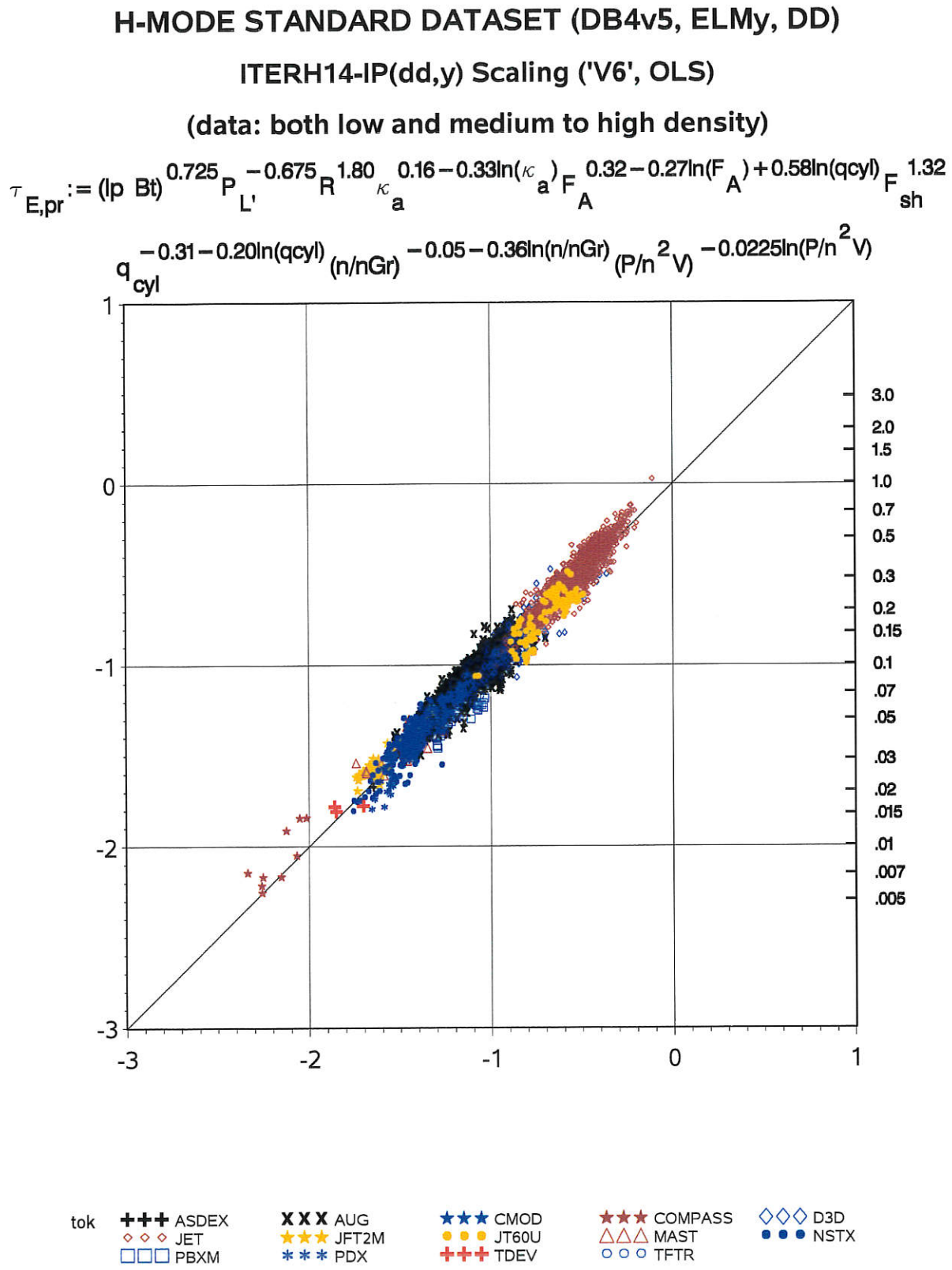

Figure 8: Observed versus fitted values of the thermal energy confinement time in s for the interaction-type scaling 'H14y' (D into D) as given by Eq. (1) in the text. This scaling is based on medium and high density discharges only. However, also low to medium density discharges have been included in the plot. This adds data from COMPASS (4 ECH and 5 ohmic H–mode) as well as from T–10 (4 ECH H–mode time-slices), and increases the total number of observations to 3543.

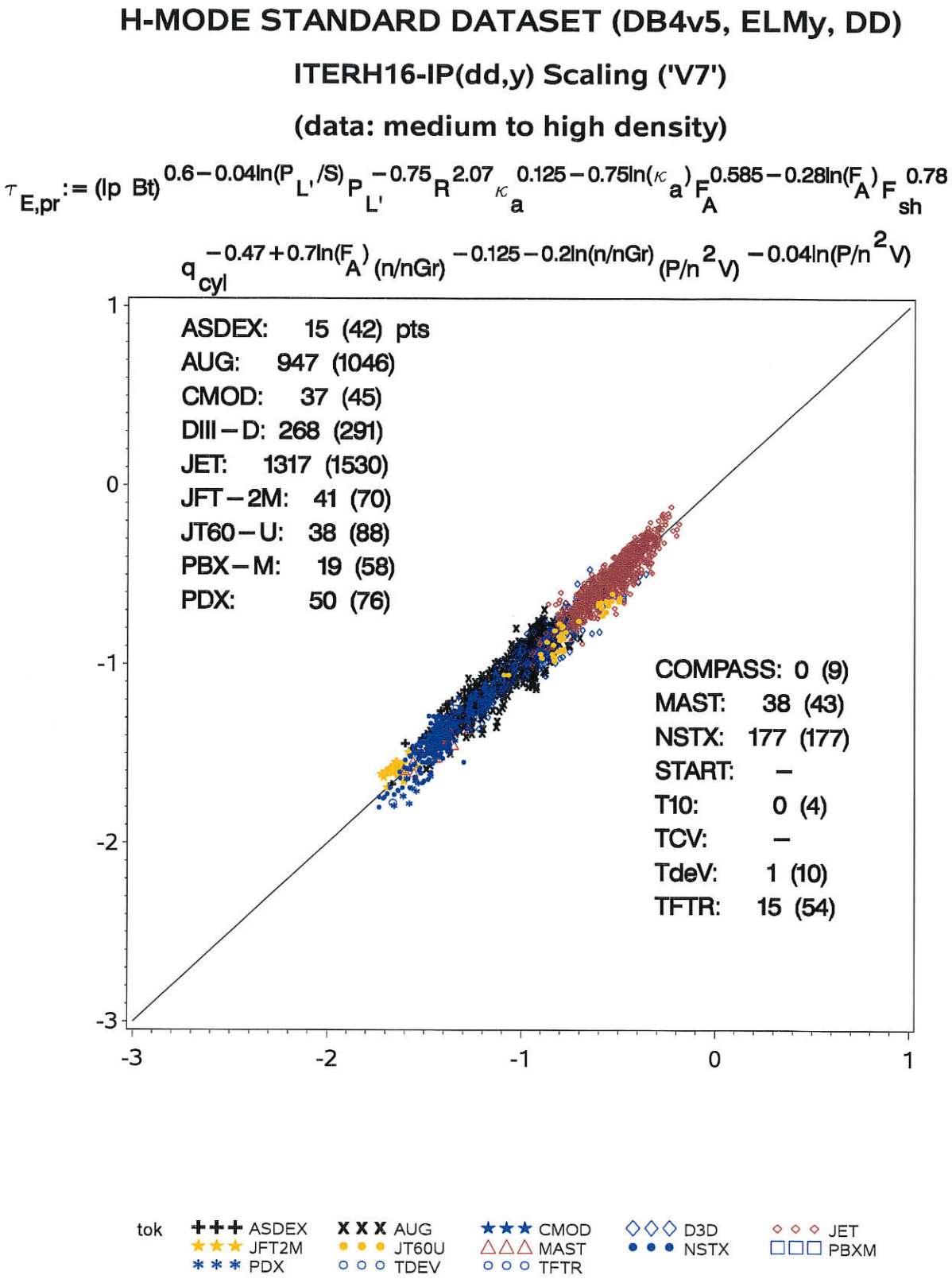

Figure 9: Observed versus fitted values of the thermal energy confinement time in s for the interaction-type scaling 'H16(y)' (D into D) as given by Eq. (2) in the text, for medium to high densities only ($N_{tok} = 13$, $N_{obs} = 2963$).

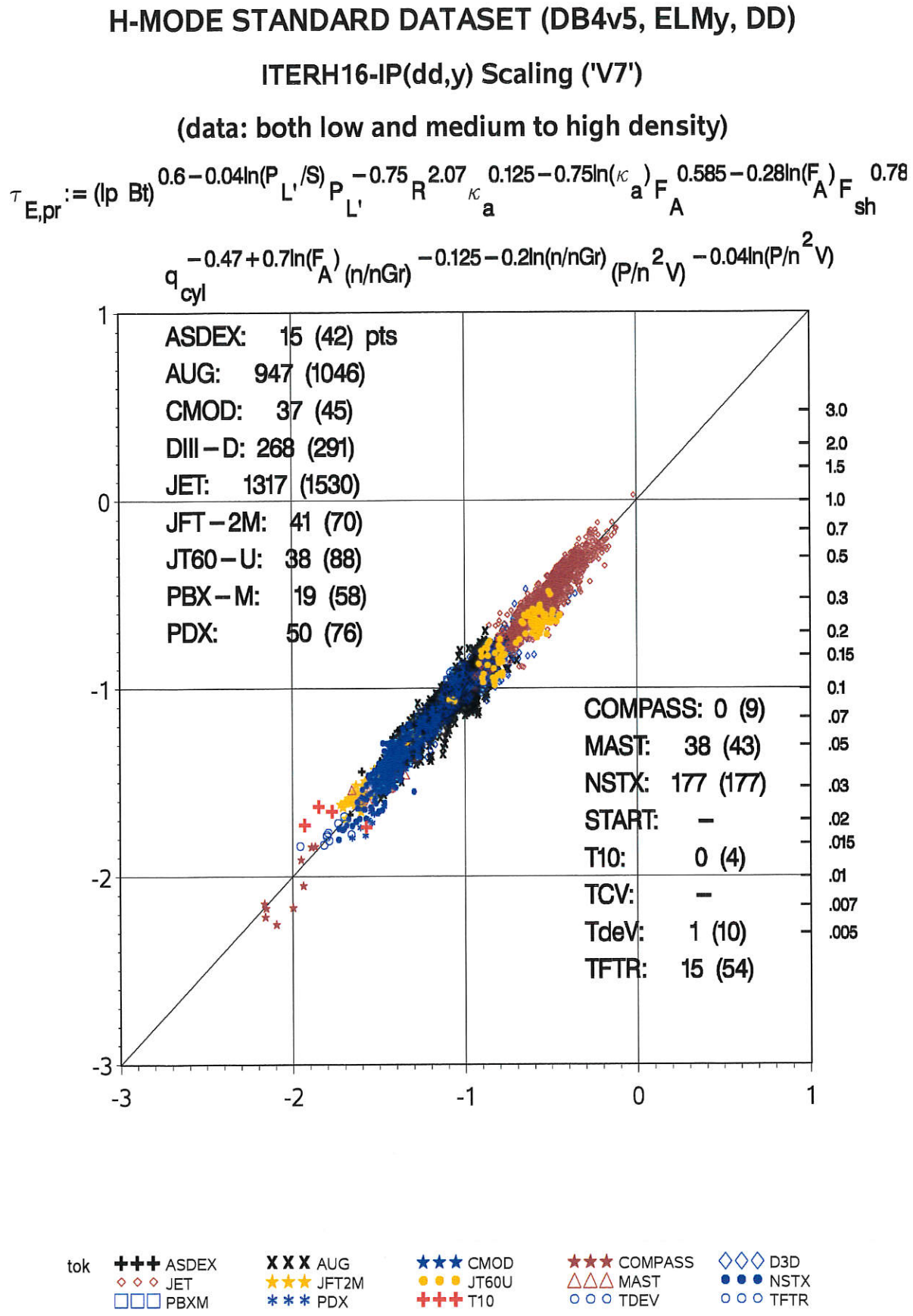

Figure 10: Observed versus fitted values of the thermal energy confinement time in s for the interaction-type scaling 'H16y' (D into D) as given by Eq. (2) in the text, for extended dataset ($N_{tok} = 15, N_{obs} = 3543$), including low densities and relaxing the constraint $0.4 < T_e/T_i < 2.5$, as in Fig. 8.

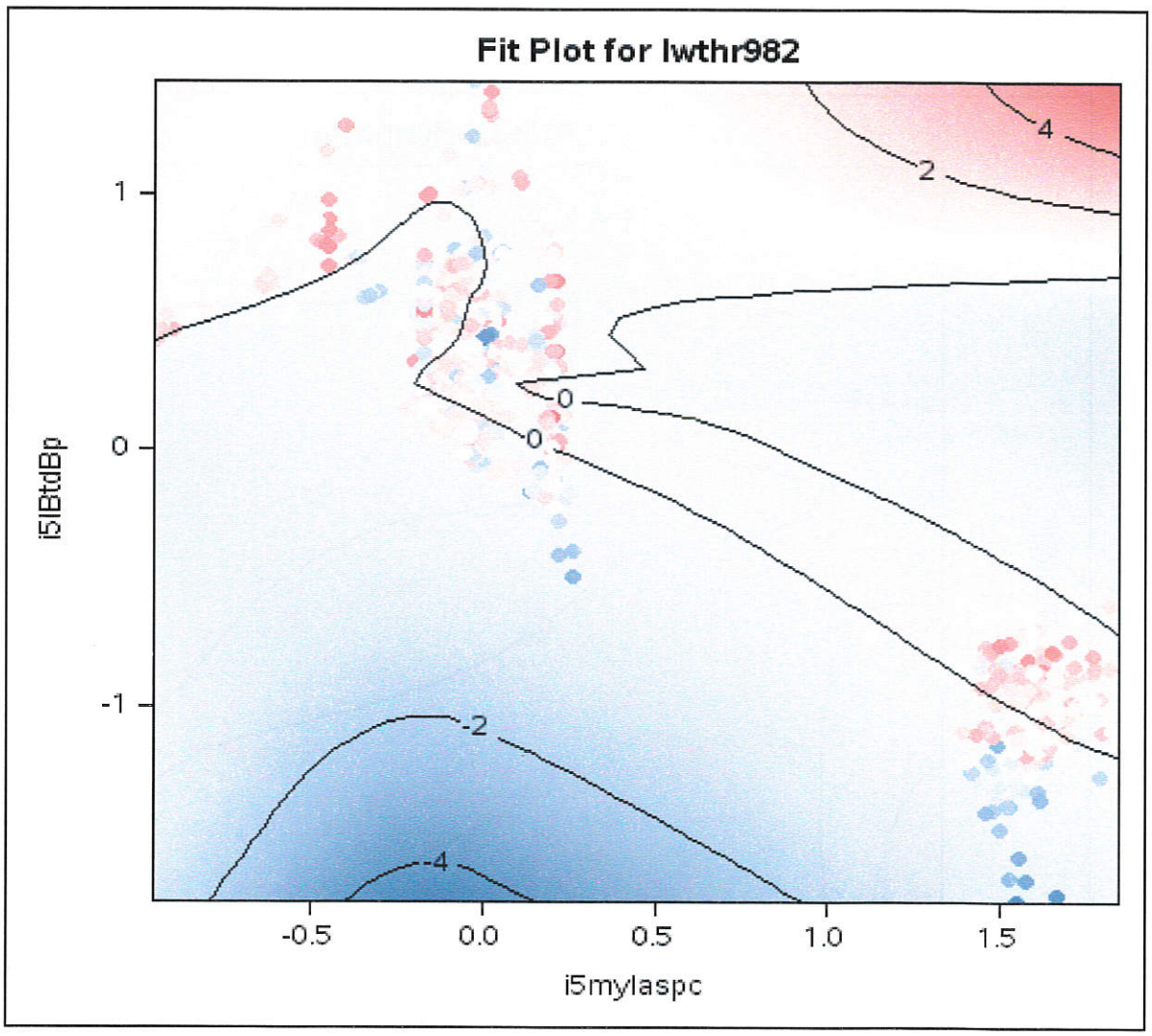

Figure 11: Residuals of $\ln \mathrm{H}_{98,y2}$ as a function of $\ln(B_t/\langle B_p \rangle)$ (vertical) and $\ln 2.0/(A-1) = \ln(B_{max}/B_{min} - 1)$ (horizontal). The origin has been shifted to the reference operating point of ITER FEAT (2003). A standard data-set selection of ITERH.DB4v5 has been used with data from 14 machines, including PBX/M (with high $A = R/a$, and an indented plasma) on the l.h.s., and MAST/NSTX (with low A) on the right. The impression that a low aspect ratio (in addition to a strong magnetic field) would be a necessary requirement to obtain a high H-factor is partly balanced by the presence of a relatively small number of observations with $\ln \mathrm{H}_{98,y2} \geq 0$, primarily related to PBX–M and circular ASDEX (now HL–2A, see [16, 17, 121]), at high aspect ratio.

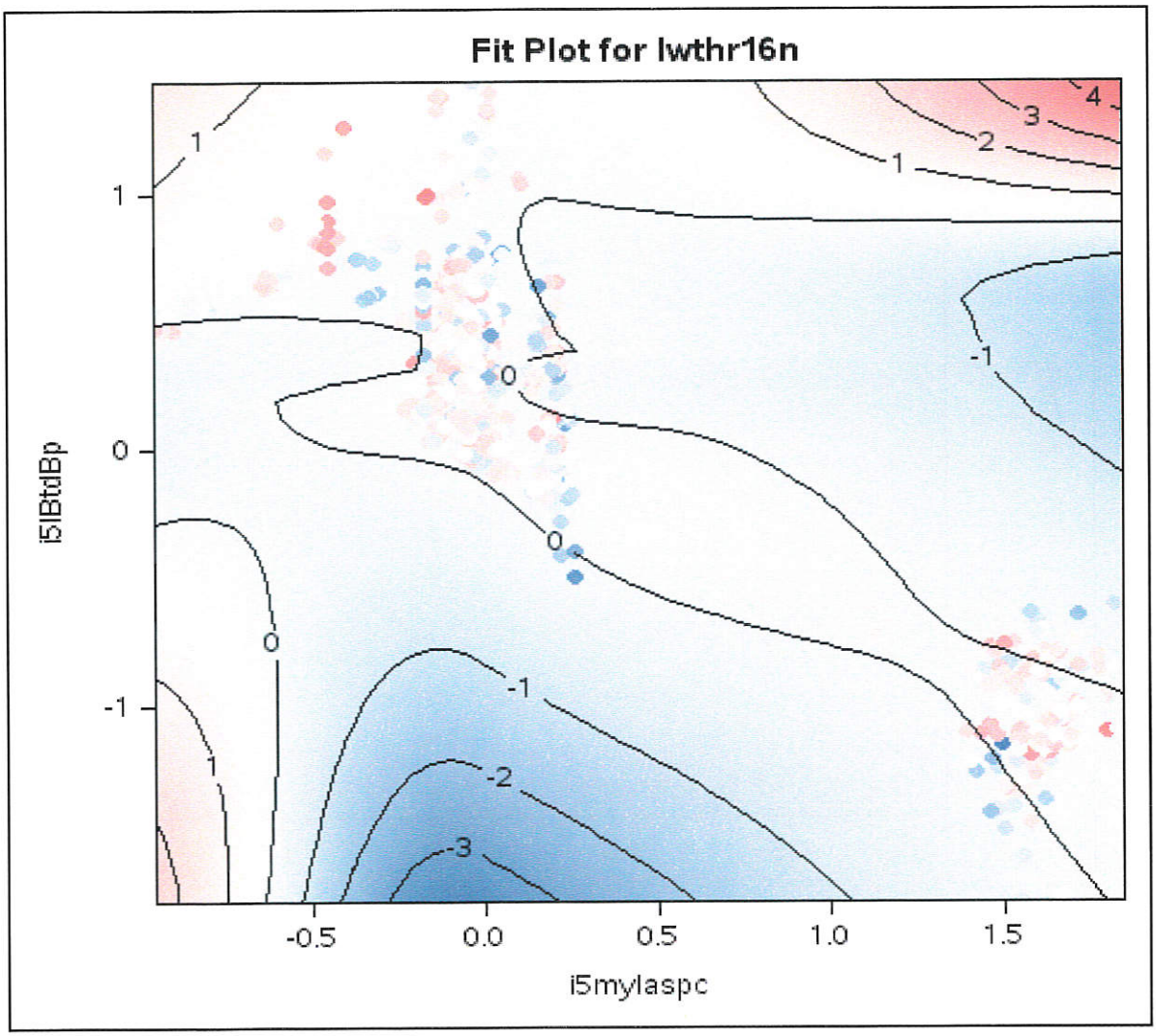

Figure 12: Residuals of $\ln \mathrm{H}_{16}$(dd,y;th) ('ITER-type' interaction scaling), as a function of $\ln(B_t/\langle B_p \rangle)$ (vertical) and $\ln 2.0/(A-1) = \ln(B_{max}/B_{min}-1)$ (horizontal). The same dataset has been used as in Fig. 11. This more refined scaling leads to a smaller systematic variation of the residuals than the scaling $\mathrm{H}_{98}(y,2)$.

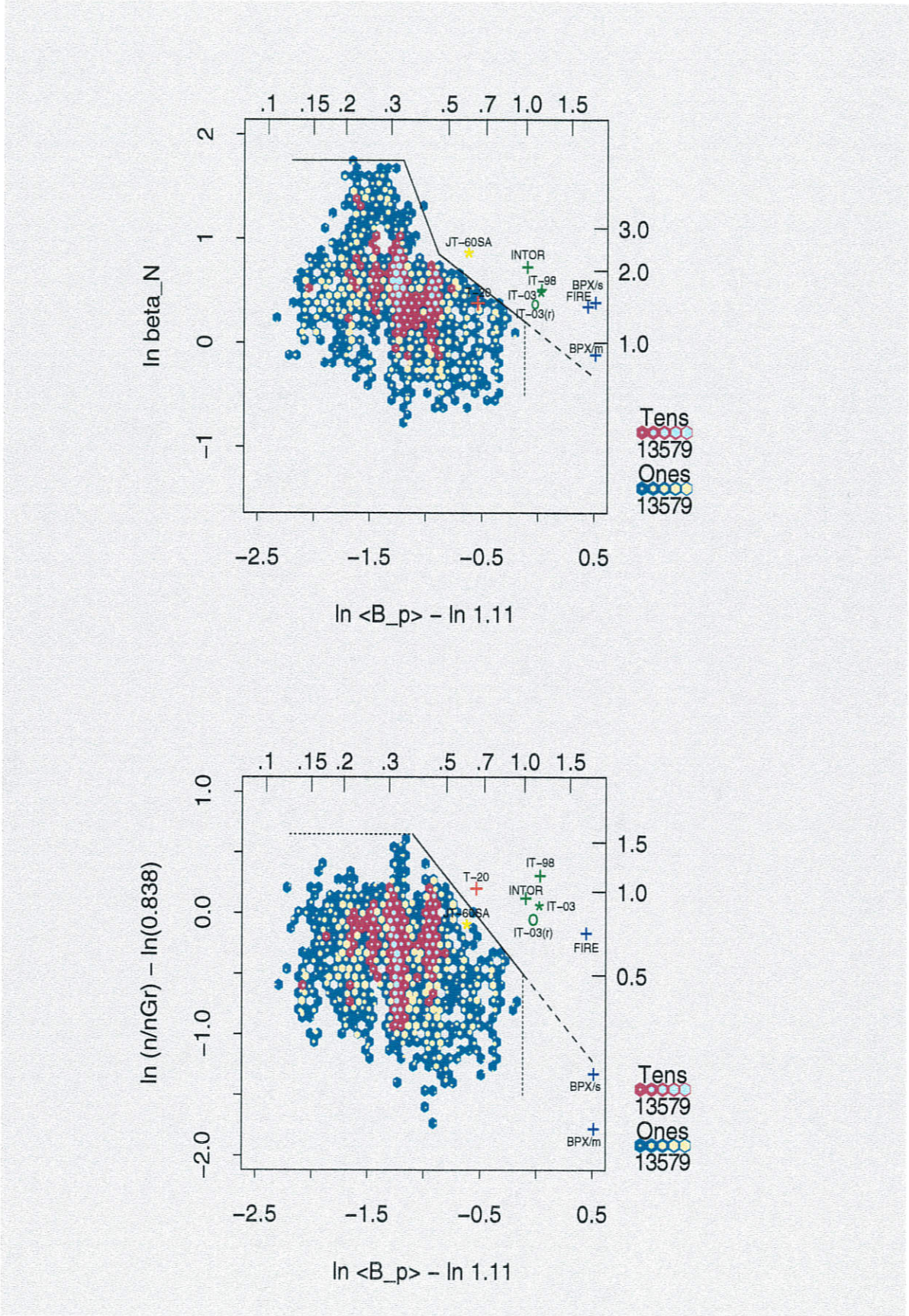

Figure 13: Same legend as in Fig. 1, now with spherical tokamaks (MAST and NSTX) included. It is a somewhat intriguing question whether the upper envelope of the achievable β_N at high current density is better represented by a log-linear polygon than by, for instance, a quadratic function.